공학박사 학위논문

High-Efficiency White & Green Organic Light-Emitting Diodes Utilizing New Dopants & Exciplex

새로운 도판트와 엑시플렉스를 이용한 고효율의
백색 및 녹색 유기발광다이오드 연구

2012년 8월

서울대학교 대학원
재료공학부
박 영 서

Abstract

High-Efficiency White & Green Organic Light-Emitting Diodes Utilizing New Dopants & Exciplex

Young-Seo Park
Department of Materials Science and Engineering
The Graduate School
Seoul National University

This thesis is composed of two parts; (1) efficient and color-stable WOLEDs using new green dopants possessing higher lowest unoccupied molecular orbital (LUMO) and highest occupied molecular orbital (HOMO) levels than the host material, and (2) utilization of exciplex forming systems for efficient OLEDs.

The fabrication of efficient and color stable white organic light emitting diodes (OLEDs) using newly synthesized yellowish green dopants are described in chapter 2. The OLEDs have a structure of multi emitting layers

(EMLs) consisting of blue, green and red EMLs in sequence. Iridium(III)bis[(4,6-difluorophenyl)-pyridinato-N,C2']picolinate (Firpic) was used as the blue dopant, newly synthesized tris-*fac*-(2-cyclohexenylpyridine) iridium(III) [$Ir(chpy)_3$] or tris-*fac*-[2-(3-methylcyclohex-1-enyl)pyridine] iridium(III) [$Ir(mchpy)_3$] as the green dopants and tris[1-phenylisoquinolinato-C2,N]iridium(III) ($Ir(piq)_3$) as the red dopant. The devices showed high efficiency with low roll off in efficiency. The maximum external quantum efficiency, luminance efficiency, and power efficiency of the WOLEDs were 11.7%, 23.4 cd/A and 13.2 lm/W, respectively. The external quantum efficiency of these WOLEDs remained high of 8.5% even at a high luminance of 10,000 cd/m^2 (~ 50 mA/cm^2). The WOLEDs showed white emission with Commission Internationale de l'Eclairage (CIE) chromaticity coordinates (0.38, 0.44) at 1,000 cd/m^2, and color variations were less than (0.02, 0.01) between 10 cd/m^2 and 5,000 cd/m^2. The WOLEDs showed color temperature about 4,300 K and CRI over 87, which are appropriate to indoor lighting application. We interpret the high color stability of the WOLEDs based on the HOMO and LUMO level alignment of the middle green dopant against the host, which controls the recombination current in each layer to be maintained in the same proportion.

Chapter 3 describes that exciplexes are easily formed at the interface

between the CBP and the bis-4,6-(3,5-di-3-pyridylphenyl)-2-methylpyrimidine (B3PYMPM), which are widely used as the EML host and the electron transporting layer (ETL) for high efficiency OLEDs, respectively. The intensity of the exciplex emission is almost proportional to the inverse square of the *fac*-tris(2-phenylpyridine) iridium [$Ir(ppy)_3$] concentration of the EML. Meanwhile, the efficiency of the OLEDs increases as the concentration of the $Ir(ppy)_3$ increases. This enhancement of the efficiency and the decrease of the exciplex emission with increasing dopant concentration originate from the increase in the energy transfer rate from the exciplex at the interface to the dopants in EML due to the decrease in the distance between the exciplex and the dopant. The energy transfer processes were successfully analyzed using the Förster energy transfer mechanism. The high-efficiency OLEDs were obtained through the energy transfer from the exciplex to the dopant at the EML/ETL interface. The EQE of the OLED reaches 20.1% when the concentration of the $Ir(ppy)_3$ is 6 mol%. In addition, we investigated the relationship between the efficiency roll-off of the OLEDs and the energy transfer from the exciplex to the dopant by inserting a thin, undoped CBP layer at the EML/ETL interface.

The exciplex can be considered as the intermolecular donor-acceptor system. Therefore the exciplex has the potential to have a small energy

difference between the singlet and triplet excited states, enabling efficient reverse intersystem crossing from the triplet charge-transfer (CT) states to the singlet CT states. This characteristic can be utilized to harvest triplet excited states for electroluminescence using fluorescent molecules via reverse intersystem crossing. Chapter 4 reports efficient triplet harvesting through exciplexes using a fluorescent molecular system composed of the 4,4',4''-tris(N-carbazolyl)-triphenylamine (TCTA) and B3PYMPM. The material system forms the exciplexes efficiently and shows the efficient delayed fluorescence emission. The delayed emission increased as the temperature decreased. As a result, the photoluminescence efficiency increased from 36% at room temperature (RT) to almost 100% at 35 K, and the external quantum efficiency of the organic light emitting diodes using the material system increased from 3.1% at RT to 10% at 195 K, clearly demonstrating that a large proportion of the triplet exciplexes are converted to light in the system. Time resolved photoluminescence spectra and transient PL of the TCTA-B3PYMPM exciplex at various temperatures indicated that the singlet and triplet exciplex have broad energy level distributions and the energy difference between them is very small, facilitating easy reverse intersystem crossing from the triplet exciplex to the singlet exciplex.

Small energy difference between the triplet and singlet exciplexes was

utilized to fabricate OLEDs with ultimate efficiencies in terms of the EQE, driving voltage, and efficiency roll-off, where exciplex-forming donor and acceptor molecules were used as the co-host of the EML (Chapter 5). The co-host system removes the charge injection barrier from the charge transporting layers to the emitting layer because the co-host materials themselves are used as the transporting materials. This exciplex forming co-host system also enables efficient singlet and triplet energy transfer from the host exciplex to the phosphorescent dopant because the singlet and triplet energy of the exciplex are almost identical. Therefore, the OLEDs achieved a low turn-on voltage of 2.4 V and a very high EQE of 29.1%. Also, due to the low driving voltage and high EQE of the OLEDs, an ultimate power efficiency level of 120.0 lm/W was recorded. In addition, the OLEDs achieve very low efficiency roll-off due to low polaron density and low triplet-triplet annihilation rate of the exciplex-forming co-host system. The EQE of the optimized OLED is maintained at more than 27.8% up to 10000 cd/m^2.

Contents

List of Tables

List of Figures

Chapter 1. Introduction

1.1 Organic Light-Emitting Diodes

Light-emitting diodes (LEDs) are devices using electroluminescence (EL) phenomenon which is light emission caused by an electrical power source. The first LED had been born in the early 20th century, and since then, LEDs have undergone a significant improvement. The Inorganic LEDs are generally based on p-n junctions of inorganic compound semiconductors, such as GaAs, GaP, GaN, AlGaAs, GaAsP, GaInN, and AlGaInP. However, the inorganic LEDs require complicated manufacturing processes, such as chemical vapor deposition (CVD) and vapor-phase epitaxy (VPE), and high-priced substrates, such as sapphire and GaP, for epitaxial growth of the inorganic semiconductors.[1] Therefore, production cost of the inorganic LEDs is high and fabrication of the inorganic LEDs with large area is very difficult.

The breakthrough was the discovery of electroluminescence of organic conjugated molecules and organic light-emitting diodes (OLEDs). In 1963, electroluminescence from an organic single crystal was firstly manifested by Pope *et al.*[2] and in 1987, Tang *et al.*[3] firstly demonstrated a vapor-deposited and double-layered OLED consisting of a hole transporting layer (HTL) and

an emitting layer (EML).[4] After that, the OLEDs have been developed noteworthily during last several decades. Based on typical characteristics of the organic materials variety processing techniques for the OLEDs are developed, such as thermal evaporation,[3] spin coating,[5] ink-jet printing,[6] screen printing,[7] and roll-to-roll printing.[8] Also, the OLEDs can be fabricated onto various substrates, such as glass,[3] polymer film,[9] and metal foil.[10] These properties of the OLEDs make lower production cost and enable large area and flexible devices.

The applications of the OLEDs are very variety. Among them, the OLEDs are most successfully applied in display industry. The OLEDs can be very thin and light weight flat panel displays. Pixels of the OLED displays directly emit light, contrary to LCDs which are using backlights. Therefore, the OLEDs enable great contrast ratio and very fast response time. Also, the OLEDs have very wide viewing angle.[11] Such advantages of the OLEDs lead extensive researches on the OLEDs. As a result, new types of the OLED displays are developed, such as flexible, rollable, and transparent OLED displays. Besides these applications, the OLEDs can be applied on solid state lighting and signage. Figure 1.1 shows examples of these applications of the OLEDs. This achievement of the OLEDs demonstrates the potential and the wide use of the OLEDs.

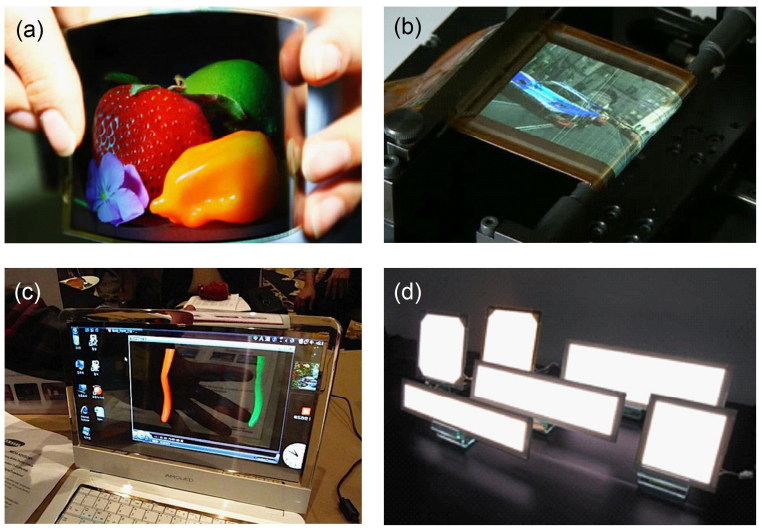

Figure 1.1 Examples of the application of the OLEDs. (a) Flexible OLED display (SMD 2011). (b) Rollable OLED display (Sony 2010). (c) Transparent OLED display (SMD 2010). (d) OLED lightings (Philips 2011).

1.2 Operation Principles of Organic Light-Emitting Diodes

1.2.1 Basic Structure and Operation of Organic Light-Emitting Diodes

The basic structure of a typical multi-layer OLED is shown Figure 1.2a which is composed of substrate / transparent anode / hole transporting layer (HTL) / emitting layer (EML) / electron transporting layer (ETL) / reflective cathode. Single-layer OLEDs are also possible, but appropriate multi-layer structure can enhance the performance of the devices by lowering the barrier for charge injection from the electrodes.[12] Therefore, multi-layer structures are generally used for the OLEDs.

Figure 1.2b shows schematic diagram of basic operation of the typical OLEDs. When during operation, a voltage is applied across the OLEDs and triangular barriers for both hole penetration into the HTL from the anode and electron penetration of the ETL from the cathode are created. The holes injected from the anode to highest occupied molecular orbital (HOMO) level of the HTL and the electrons injected from cathode to lowest unoccupied molecular orbital (LUMO) level of the ETL. In the low-current carrier injection regime, the current is determined by the rate at which charge hops over the barriers or

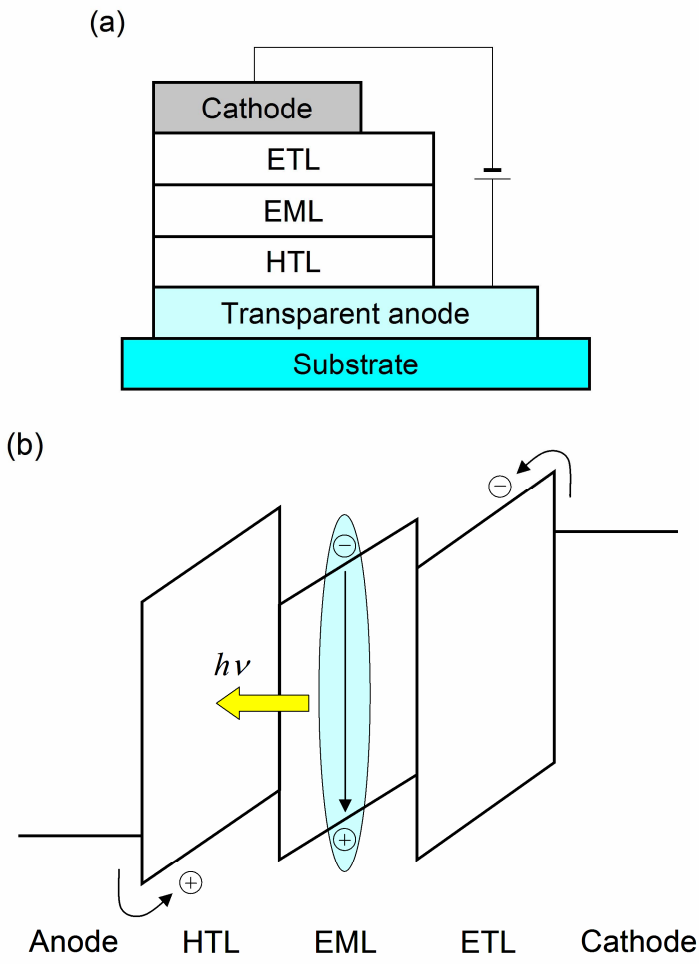

Figure 1.2 (a) The basic structure of the typical multi-layer OLED. (b) The schematic diagram of basic operation of the typical OLEDs.

is transported through the barrier. In the high-current space-charge limited current (SCLC) regime, the current is determined by the intrinsic properties of the layers through which it flows. Unlike inorganic semiconductors, the transport properties in the OLEDs are determined by intersite hopping of charge carriers between localized states.[12]

When the hole and the electron approach, Electrostatic forces bring the electrons and the holes towards each other and they recombine forming an exciton. Then, emission is occurred by emissive transition from the excited states to ground states. This happens typically in the EML. The energy of the emitted light depends on energy gap of the emitting material.

Types of the EML can be roughly divided into two types; neat film type and host-dopant type. The host-dopant type EML is a blended layer with high concentration of host molecules and low concentration of dopant molecules. In a solid state, emission efficiency can be reduced by concentration quenching. Therefore, the doping of highly efficient molecules into the EML contributes the enhancement of the emission efficiency of the OLEDs.[12] The host molecules have wider energy gap than dopant molecules. The excitation energy of the host molecules can be transferred to the dopant molecules through Föster energy transfer or Dexter energy transfer, and then the dopant molecules emit the light. The Föster energy transfer is energy transfer through

the dipole-dipole interaction and the Dexter energy transfer is direct quantum mechanical electron transfer.[13] Figure 1.3 shows schematic diagram of Föster and Dexter energy transfer process. Typically, singlet excitons are generally transferred by Föster energy transfer and triplet excitons are generally transferred by Dexter energy transfer.

1.2.2 Characteristics of Organic Light-Emitting Diodes

The efficiency is a key issue for energy-consumption of the OLEDs. For OLEDs, much of analysis of the efficiency has been devoted to the external quantum efficiency (EQE) which means number of photons emitted through the front face of the device per injected electron. The basic equation for the EQE of the OLEDs can be written is

$$\eta_{EQE} = \eta_{out}\eta_{re}\chi\eta_{PL}, \quad (1)$$

where η_{EQE} is the EQE of the OLEDs, η_{out} is outcoupling efficiency which means the fraction of the photons extracted through the front face of the device, η_{re} is the ratio of the number of exciton-forming events to the electrons flowing in the external circuit, χ is the ratio of excitons which is possible to emit, and η_{PL} is the PL quantum yield.[12]

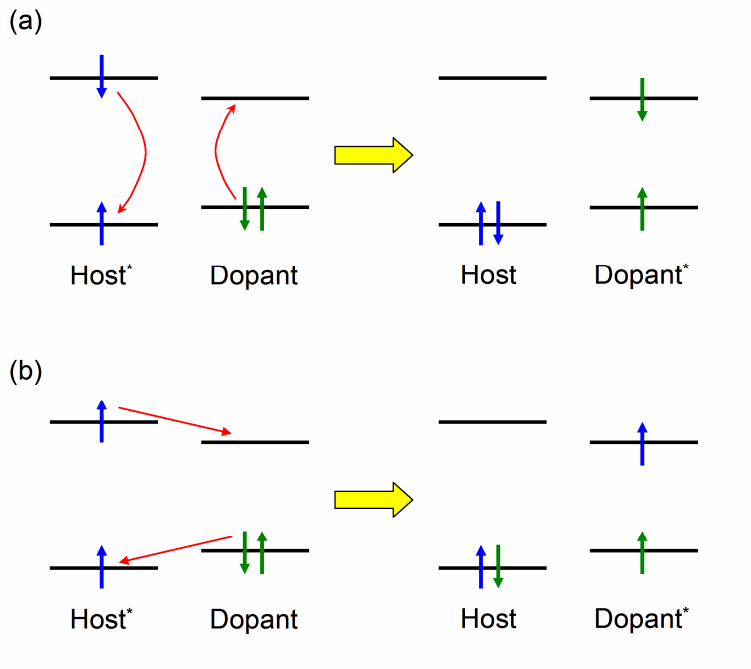

Figure 1.3 The schematic diagram of (a) Föster and (b) Dexter energy transfer process.

Until several years ago, it was generally recognized that η_{out} of the bottom emission OLEDs are limited about 20%. However, recently published paper reports that η_{out} of the bottom emission OLEDs can achieve about 30% when optical condition is optimized.[14] The factor η_{re} is a measure of the balance between the hole and the electron injection. When the injected hole and electron are balanced, η_{re} can be close to 1. In the fluorescent OLEDs, only singlet exciton can emit light, therefore χ of the fluorescent OLEDs is typically 0.25 due to spin-statistics ratio between singlet and triplet. However, χ of the phosphorescent OLEDs is 1 because triplet exciton can emit light in the phosphorescent OLEDs. η_{PL} is a material property. Many efficient emitting materials achieved 100% of η_{PL}.[12] Considering all the factors mentioned above, the limit of the EQE of the phosphorescent bottom emission OLEDs is about 30%.

The driving voltage is also important factor which influence power consumption of the OLEDs. The driving voltage of an OLED must be composed of the voltage corresponding to the emitting photon energy ($V = E_{photon} / q$, where V is the voltage, E_{photon} is the photon energy of the emitted light and q is the unit charge) and the over-potential required to inject and transport electrons and holes from the electrodes to the emitting layer

(EML), where the electrons and holes recombine. Therefore, the low limit of the driving voltage close to the voltage corresponding to the photon energy of the light emitted of the OLED.

1.3 White Organic Light-Emitting Diodes

1.3.1 Structures of White Organic Light-Emitting Diodes

To obtain white light, several colored light should be mixed; three primary colors or two complementary colors. Since the first reports of white organic light-emitting diodes (WOLEDs) by Kido *et al.*[15] many approaches to generating white light from the OLEDs have been developed. Among them, single-EML structure,[15] multi-EML structure,[16] and tandem structure[17] are most popular structures of WOLEDs. (Figure 1.4)

The Single-EML WOLEDs emit white light from a single EML. To ensure that white light emission from the single EML, generally several dopants mixed into a single host layer. The Single-EML WOLEDs have simple structure, so relatively easy to fabricate. However, it is very difficult to control the doping ratio between the each dopant materials to attain balanced white emission.[18]

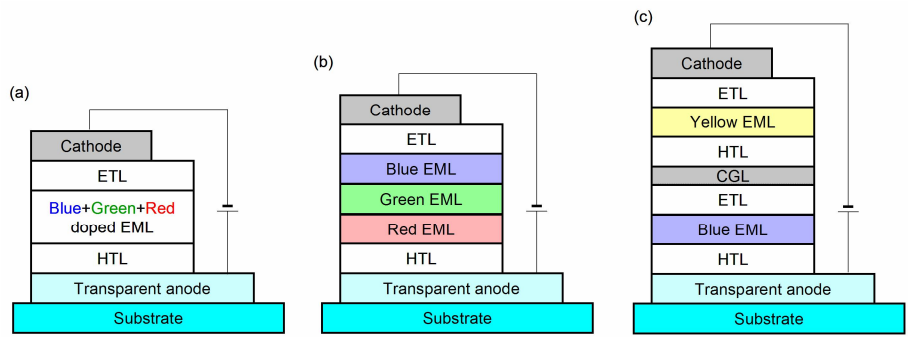

Figure 1.4 The schematic diagram of the typical structure of (a) the single-EML WOLED, (b) the multi-EML WOLED, and (c) the tandem WOLED.

In the multi-EML WOLEDs, several EMLs are employed to emit each color simultaneously. In this structure, position of the recombination zone in the EMLs is important factor to balance white light. The recombination zone can be controlled by introducing charge blocking layers, by varying layer thickness, and by adjusting dopant concentrations.[19]

The tandem WOLEDs comprise two or more complete stacked OLED units layered on top of each other with charge generation layers (CGLs) between them. The tandem WOLEDs can obtain white emission either through multiple white units or by individual color units. Generally, the tandem WOLEDs can achieve high EQE and long lifetime. However, they have complicated structures and require very high driving voltage.[18]

Besides these structures, there are many methods to fabricate the WOLEDs, for example, down conversion WOLEDs, WOLEDs using excimer or exciplex, and WOLEDs employing multimode resonant cavities.[19]

1.3.2 Characteristics of White Organic Light-Emitting Diodes

The WOLEDs attract much attention in recent years due to their potential use in solid state lighting applications and flat panel displays. However, there are many requirements for these commercial applications. They include

requirements of the general OLEDs, such as high efficiency, low driving voltage, and long lifetime, and characteristic requirements for WOLEDs, such as proper color coordinates and color temperature, high color rendering index (CRI), and high color stability.[20]

The color coordinates are numbers which used specify color of light. The color coordinates of equi-energy white light are (0.33, 0.33). The color temperature is related to the color coordinates of the calculated black body spectrum $BB(\lambda)$ at a specific temperature using following equation:

$$BB(\lambda) = \frac{c_1}{\lambda^5[\exp(c_2 / \lambda T) - 1]}, \quad (2)$$

where c_1=3.74×10^{-16} (W/m^2) and c_2=1.44×10^{-2} (m K). Doing this for everh color temperature maps out the 'blackbody locus' in the color space as depicted in Figure 1.5. A lower color temperature corresponds to a 'warmer' light and a higher color temperature corresponds to a 'colder' light. For general illumination, it has been found that the preferred white light colors are light with the color temperature between 2800 ~ 6500 K.[21]

The CRI is a quantitative measure of the ability of a light source to reproduce the colors of various objects faithfully in comparison with an ideal or natural light source. For a given light source, the CRI attempts to quantify how different a set of test colors appears when illuminated by the source compared

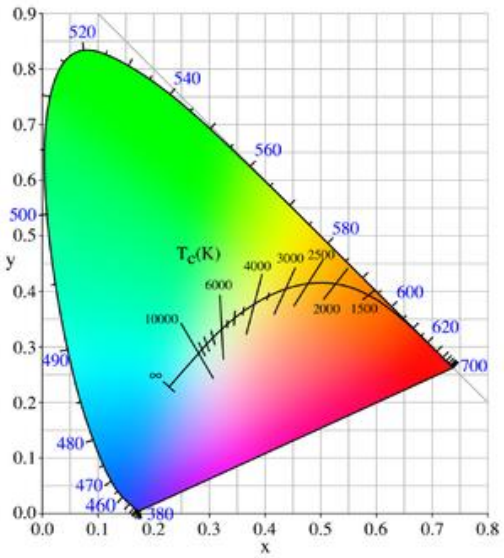

Figure 1.5 The blackbody locus in the CIE 1931 color space.

to when the same test colors are illuminated by the standard illuminant with the same correlated color temperature. The difference in the rendering of the test color between the two light sources can be quantified (ΔE). The final calculation of the CRI involves calculating ΔE for well-defined eight test colors and then averaging according to following definition:

$$CRI = R_a = 100 - 4.6\sum_{i=1}^{8} \frac{\Delta E_i}{8}, \quad (3)$$

where the index refers to the different test colors. Achieving illumination-quality white light generally requires the CRI value over than 80.[21]

Generally, WOLEDs includes several kinds of emitting materials which emit different colors. In this case, different dopants can conceivably compete with one another under different driving conditions due to differences in the exciton energy and shifts in the recombination zone. As a result, the color performance will vary with different driving conditions, luminance levels and degrees of device degradation. For lighting applications, color variation during operation will distort the color of the illuminated object. For display applications, the panel will suffer from distortions of the pixel emitting color and non-uniform color distribution over the panel. Therefore, for competitiveness in the market, WOLED must be developed with high color stability.[22]

1.4 Exciplex in Organic Light-Emitting Diodes

An electronically excited state may participate in charge-transfer interactions with other molecules. As a result, a complex between an electronically excited molecule, M^*, with other ground state molecule, N, can be stabilized by charge-transfer interaction. This complex, $(MN)^*$, is new electronically excited species and it is termed an exciplex.[23]

The enhanced stabilization of the exciplex can be understood from two factors. The one factor is energy level difference between the electron donor molecule and the electron acceptor molecule. If the acceptor molecule has lower HOMO and LUMO level than the donor molecule, the exciplex will be stabilized than the exciton state as much as energy level difference between the two molecules.[24] The other factor is molecular orbital interaction. According to the rules of perturbation theory, HOMOs and LUMOs of the both molecules will interact to split and to form new two HOMOs and LUMOs when two molecules brought into contact. Since one of the molecules is electronically excited, three electrons are stabilized and only one electron is destabilized from their original non-interacting orbitals to the new orbitals of the exciplex.[23] Figure 1.6 shows schematic diagram of the molecular orbital interactions in exciplex.

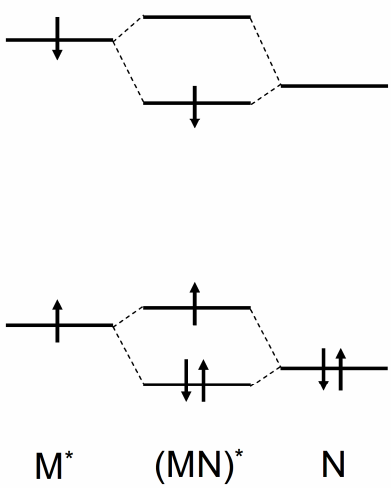

Figure 1.6 The schematic diagram of the molecular orbital interactions in exciplex.

Figure 1.7 shows a schematic potential-energy surface description of the exciplex formation. When ground state molecules, M and N, approach, steric hindrance will repel the molecules since there are no attractions between M and N. However, when one of the molecules is excited (M^* and N), the bonding between them may increase as the two molecules approach due to charge transfer and excitation exchange interactions. This will cause minimum in the potential-energy curve.[23]

The multi-layer structure is general structure of the OLEDs because multi-layer structure has advantages on the injection of the charge carriers and the exciton confinement in the EML. The charge blocking energy barriers at the interface between the EML and the neighboring layer confine the charges in the EML and enhance recombination in the region close to heterojunction. However, this heterojunction also promotes the formation of the exciplexes. The difference in energy levels of the two materials constituting the heterojunction is the primary factor governing exciplex formation.[24] Figure 1.8 shows schematic diagram of the exciplex formation at the heterojunction of the OLEDs.

The exciplex emission is red-shifted with respect to the emission of the each molecule. This is related to the energy difference between the HOMO level of the donor material and the LUMO level of the acceptor material, which favors

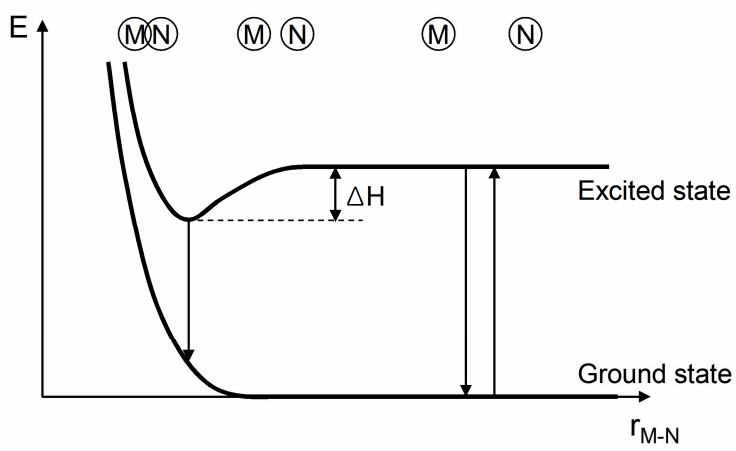

Figure 1.7 The schematic potential-energy surface description of the exciplex formation.

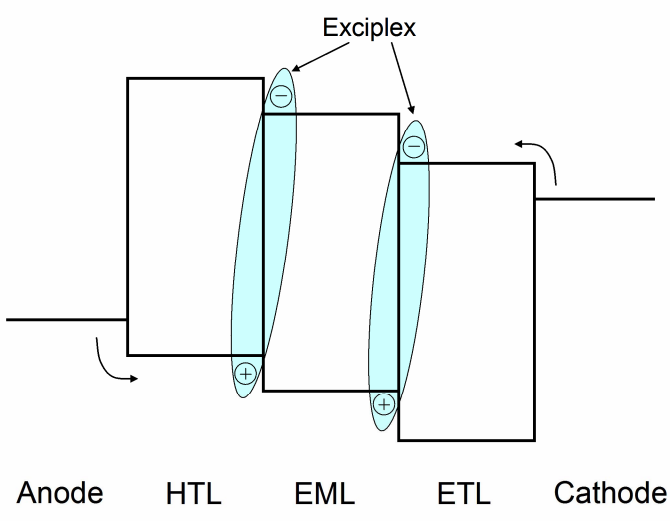

Figure 1.8 The schematic diagram of the exciplex formation at the heterojunction of the OLEDs.

generation of bound states of lower energy rather than excitons.[24] Also, the formation of the exciplex generally leads to broadened spectrum relative to the emissions of the individual donor or acceptor. It is because there may be relaxation from locally excited state to the exciplex state prior to emission.[25] The radiative decay time is observed to be generally longer for the exciplexes than for the excitons[26] and the emission efficiency of the exciplex generally lower than the excitons.[27]

1.5 Outline of thesis

In this thesis, efficient and color-stable WOLEDs using the new dopant which have higher energy levels than the host material are reported. Also, the harvesting mechanisms of the exciplex to the light emission are investigated based on the energy transfer and the reverse intersystem crossing (RISC), and the efficient OLEDs are developed utilizing these mechanisms.

The mechanism of color stability enhancement of the WOLEDs is investigated by paying attention to the energy level difference between the host and the dopant. The high energy level of the dopant impedes movement of the charge carriers, and enhances color stability and efficiency of the OLEDs. (Chapter 2)

The energy transfer from the exciplex to the dopant is analyzed by Förster energy transfer mechanism. The intensity of the exciplex emission is controlled by distance between the exciplex to the dopant. The efficiency reduction by the exciplex can be reduced by the energy transfer of the exciplex to the dopant. (Chapter 3)

Efficient triplet harvesting using the RISC of the TCTA-B3PYMPM exciplex is demonstrated. The enegetics of the exciplex is analyzed based on transient PL and time resolved PL spectrum of the exciplex. The EQE of the OLED reached to 10% at 195 K by the triplet exciplexes harvesting. (Chapter 4)

The phosphorescent OLEDs with extremely low driving voltage, high efficiency, and a low efficiency roll-off were realized using an exciplex-forming co-host. The exciplex forming co-host system reduces the charge injection barrier from the charge transporting layers to the EML and allows an efficient energy transfer from the exciplex to the dopant. The co-host system distributes the recombination zone all over the EML and reduces the triplet exciton quenching process. (Chapter 5)

1.6 Bibliography

1. E. F. Schubert, *Light-Emitting Diodes*, Cambridge University Press, Cambridge, UK, **2003**.
2. M. Pope, H. P. Kallmann, and P. Magnantte, *J. Chem. Phys.* **1963**, 38, 2042.
3. C. W. Tang and S. A. Van Slyke, *Appl. Phys. Lett.* **1987**, 51, 913.
4. K. Müllen and U. Scherf, *Organic Light-Emitting Devices*, Wiley-VCH, Weinheim, Germany, **2006**.
5. J. Kido, K. Nagai, Y. Okamoto, and T. Skotheim, *Appl. Phys. Lett.* **1991**, 59, 2760.
6. T. R. Hebner, C. C. Wu, D. Marcy, M. H. Lu, and J. C. Sturm, *Appl. Phys. Lett*. **1998**, 72, 519.
7. D. A. Pardo, G. E. Jabbour, and N. Peyghambarian, *Adv. Mater.* **2000**, 12, 1249.
8. P. Kopola, M. Tuomikoski, R. Suhonen, and A. Maaninen, *Thin Solid Films* **2009**, 517, 5757.
9. G. Gustaffson, G. M. Treacy, Y. Cao, F. Klavertter, N. Colaneri, and A. J. Heeger, *Synth. Metals* **1993**, 57, 4123.
10. C. C. Wu, S. D. Theiss, G. Gu, M. H. Lu, J. C. Sturn, S. Wagner, and S. R.

Forrest, *IEEE Electron. Dev. Lett.* **1997**, 18, 609.

11. M. A. McCarthy, B. Liu, E. P. Donoghue, I. Kravchenko, D. Y. Kim, F. So, and A. G. Rinzler, *Science* **2011**, 332, 570.
12. J. Shinar, *Organic Light-Emitting Devices*, Springer, New York, U.S.A, **2004**.
13. Z. Li and H. Meng, *Organic Light-Emitting Materials and Devices*, Taylor & Francis, Boca Raton, U.S.A, **2007**.
14. S.-Y. Kim and J.-J. Kim, *Org. Electron.* **2010**, 11, 1010.
15. J. Kido, K. Hongawa, K. Okuyama, K. Nagei, *Appl. Phys. Lett.* **1994**, 64, 815.
16. M. Berggren, G. Gustafsson, O. Lnganäs, M. R. Andersson, T. Hjertberg, and O. Wennerström, *J. Appl. Phys.* 1994, 76, 7530.
17. C.-C. Chang, J.-F. Chen, S.-W. Hwang, and C. H. Chen, *Appl. Phys. Lett.* **2005**, 87, 253501.
18. K. T. Kamtekar, A. P. Monkman, and M. R. Bryce, *Adv. Mater.* **2010**, 22, 572.
19. B. W. D'Andrade and S. R. Forrest, *Adv. Mater.* **2004**, 16, 1585.
20. Y.-S. Park, J.-W. Kang, D. M. Kang, J.-W. Park, Y.-H. Kim, S.-K. Kwon, and J.-J. Kim, *Adv. Mater.* **2008**, 20, 1957.
21. Z. Kafafi, *Organic Electroluminescence*, Taylor & Francis, Boca Raton,

U.S.A, **2005**.

22. C.-H. Hsiao, Y.-H. Lan, P.-Y. Lee, T.-L. Chiu, and J.-H. Lee, *Org. Electron.* **2011**, 12, 547.
23. N. J. Turro, *Modern Molecular Photochemistry*, University Science Books, Mill Vally, U.S.A, **1991**.
24. M. Castellani and D. Berner, *J. Appl. Phys.* **2007**, 102, 024509.
25. W. T. Yip and D. H. Levy, *J. Phys. Chem.* **1996**, 100, 11539.
26. A. C. Morteani, R. H. Friend, and C. Silva, *J. Chem. Phys.* **2005**, 122, 244906
27. N. Matsumoto, M. Nishiyama, and C. Adachi, *J. Phys. Chem. C* **2008**, 112, 7735.

Chapter 2. Efficient, Color Stable White Organic Light-Emitting Diode Based on High Energy Level Yellowish-Green Dopants

2.1 Introduction

White organic light-emitting diodes (WOLEDs) attract much attention in recent years due to their potential use in back light unit of flat panel displays, full color display and solid state lighting applications. The applications require WOLEDs possess high efficiency, appropriate color temperature, high color rendering index, and high color stability.[1] Various approaches have been reported to improve the performance, which include doping of several fluorophors or phosphors in a single emitting layer (EML),[2–8] synthesis of polymers incorporating different color emitting moieties,[9–11] use of excimer or exciplex formed by one or two dopants,[12–14] stacked several organic light emitting diodes (OLEDs),[15–17] use of microcavity effect from single emission layer,[18] down conversion of blue light,[1,19] and multi-EML structure doped with different color emitting dopants.[20–25] Among them, multi-EML structure has advantages over other architectures in terms of efficiency and color

controllability because the recombination current, singlet and triplet energy transfer and performance of each layer can be controlled by layer thickness, doping concentration and charge blocking layers. One drawback of the WOLEDs with multi-emissive layers is the color shift with increasing voltage.[21–25] The color shift is believed to be originated from the shift of recombination zone with increasing voltage and easier formation of high energy excitons at higher voltage.[5] In this paper, we report the fabrication of efficient, color-stable, multi-EML WOLEDs using three phosphorescent dopants; iridium(III)bis[(4,6-difluorophenyl)-pyridinato- $N,C^{2'}$]picolinate (FIrpic) as the blue dopant, newly synthesized tris-*fac*-(2-cyclohexenylpyridine) iridium(III) [$Ir(chpy)_3$] or tris-*fac*-[2-(3-methylcyclohex-1-enyl)pyridine] iridium(III) [$Ir(mchpy)_3$] as the yellowish-green dopant, and tris[1-phenylisoquinolinato-C2,N]iridium(III) [$Ir(piq)_3$] as the red dopant. N,N'-dicarbazolyl-3,5-benzene (mCP) was used as the host for blue dopant and N,N'-dicarbazolyl-4-4'-biphenyl (CBP) as the green and red host, respectively. The devices showed high efficiency with low roll off in efficiency. The maximum external quantum efficiency, luminance efficiency, and power efficiency of the WOLEDs were 11.7%, 23.4 cd/A and 13.2 lm/W, respectively. The external quantum efficiency of these WOLEDs remained high of 8.5% even at a high luminance of 10000 cd/m^2 (~ 50 mA/cm^2). The

WOLEDs showed white emission with Commission Internationale de l'Eclairage (CIE) chromaticity coordinates (0.38, 0.44) at 1000 cd/m^2, and color variations were less than (0.02, 0.01) between 10 cd/m^2 and 5000 cd/m^2. The WOLEDs showed color temperature about 4300K and color rendering index (CRI) over 87, which are appropriate to indoor lighting application. We interpret the high color stability of the WOLEDs based on the higher highest occupied molecular orbital (HOMO) and the lowest unoccupied molecular orbital (LUMO) level alignment of the middle green dopant against the host, which controls the recombination current in each layer to be maintained in the same proportion.

2.2 Experimental

The WOLEDs were fabricated by thermal evaporation onto a cleaned glass substrate precoated with indium tin oxide (ITO) without breaking the vacuum. Prior to organic layer deposition, the ITO substrates were exposed to UV-ozone flux for 10 min following degreasing in acetone and isopropyl alcohol. All layers were grown by thermal evaporation at the base pressure of $< 5\times10^{-7}$ Torr. Layers were deposited in following order: hole transporting layer (HTL) / blue EML / green EML / red EML / electron transporting layer (ETL) /

cathode. 40-nm-thick N,N'–di(naphthalene-1-yl)-N,N'-diphenylbenzidine (NPB) was used as the HTL and 20-nm-thick mCP doped with 6wt% FIrpic as the blue EML. Green EML is 5-nm-thick CBP doped with 6wt% green dopant. $Ir(chpy)_3$, $Ir(mchpy)_3$, and $Ir(ppy)_3$ were used as the green dopant for device 1, 2, and 3, respectively. 5-nm-thick CBP doped with 6wt% $Ir(piq)_3$ was used as the red EML and 40-nm-thick aluminum(III) bis(2-methyl-8-quinolinato)4-phenylphenolate (BAlq) was used as the ETL, respectively. Finally, the cathode consisting of a 1-nm-thick LiF and a 100-nm-thick layer of Al were deposited onto the sample surface. $Ir(chpy)_3$ and $Ir(mchpy)_3$ were synthesized in Gyeongsang National University. Two ligands, 2-(1-cyclohexenyl)pyridine (chpy) and 2-(3-methyl-1-cyclohexenyl)pyridine (mchpy) were prepared from 2-bromopyridine with cyclohexanone derivatives in two steps. The desired iridium complexes were synthesized according to a modified procedure reported previously.[26,27] Bis-cyclometalate Iridium complexes bearing acetylacetonate (acac) as ancillary ligand were synthesized by a conventional two-step reaction from iridium trichloride via Ir(III)-m-chlorobridged dimer complexes. The tris-cyclometalated complexes ($Ir(chpy)_3$, $Ir(mchpy)_3$) were prepared by reaction of the ligands with biscyclometalated Ir complexes in glycerol. Details of the synthesis of the materials will be described elsewhere.[28] All the materials were purified using train sublimation before use.

HOMO levels of organic materials are obtained from the cyclic voltammetry measurement, and LUMO levels are calculated from HOMO level and energy gap which is obtained from the edge of the absorption spectra. Current density–voltage–luminescence (J–V–L) characteristics of the WOLEDs were measured simultaneously using a Keithley 2400 programmable source meter and a SpectraScan PR650 (Photo Research). External quantum efficiency was calculated from the spectral luminance power in the forward direction of the WOLEDs. CRI and color temperature were calculated by CIE D008-1995.

2.3 Result and Discussion

Figure 2.1 shows the structures of the devices, and the energy levels of the materials. The molecular structures of the dopants used in this study are shown in Figure 2.1b. Three kind of devices were fabricated with different green dopants; $Ir(chpy)_3$ for device 1, $Ir(mchpy)_3$ for device 2 and fac tris(2-phenylpyridine) iridium ($Ir(ppy)_3$) for device 3, respectively. The device 3 was fabricated for comparison purposes.

Figure 2.2 displays the electroluminescent (EL) spectra of the WOLEDs at several different luminances of 10, 100, 1000, and 5000 cd/m^2. The EL spectra exhibited the peak wavelengths at 472, 536, and 620nm in the device

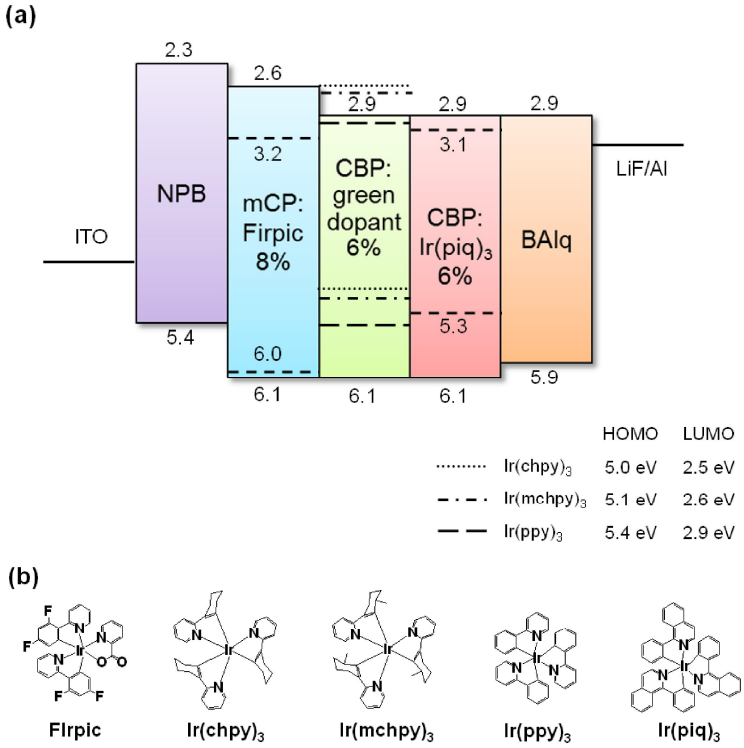

Figure 2.1 (a) Structures of the devices and energy levels of materials. (b) Molecular structures of dopants used in the study.

1 and 2. They correspond to the peak wavelengths of the EL spectra of the single color OLEDs using FIrpic, $Ir(chpy)_3$ (or $Ir(mchpy)_3$) and $Ir(piq)_3$ dopants, respectively. The EL spectra of these WOLEDs covered all wavelengths from 450nm to 750nm and were stable as the luminance varied. At 1000 cd/m^2, CRI and color temperature were calculated to reach 87.94 and 4246 K for device 1, and 87.27 and 4316 K for device 2, respectively. These high CRI's of the device 1 and 2 are originated from the similar intensity of the three emission peaks and coverage of the whole visible wavelength. In contrast, the EL spectra of the device 3 exhibited peaks at wavelengths of 472, 508, and 620 nm and very low emission near 580 nm. Therefore the device shows lower CRI of 66.13 at 1000 cd/m^2. Moreover, the relative intensity of the red peak varied significantly as the luminance increased.

CIE chromaticity coordinates of the WOLEDs at the luminance range of 10–5000 cd/m^2 are displayed in Figure 2.3. When the luminance changed from 10 cd/m^2 to 5000 cd/m^2, the CIE chromaticity coordinates of the device 1 and 2 changed less than the device 3: CIE X = 0.37–0.39 and CIE Y = 0.43–0.44 for the device 1, CIE X = 0.37–0.38 and CIE Y = 0.43–0.44 for the device 2, and CIE X = 0.35–0.38 and CIE Y = 0.39–0.42 for the device 3.

We interpret the high color stability of the device 1 and 2 based on the energy level difference between the host and the dopant of the green EML. As

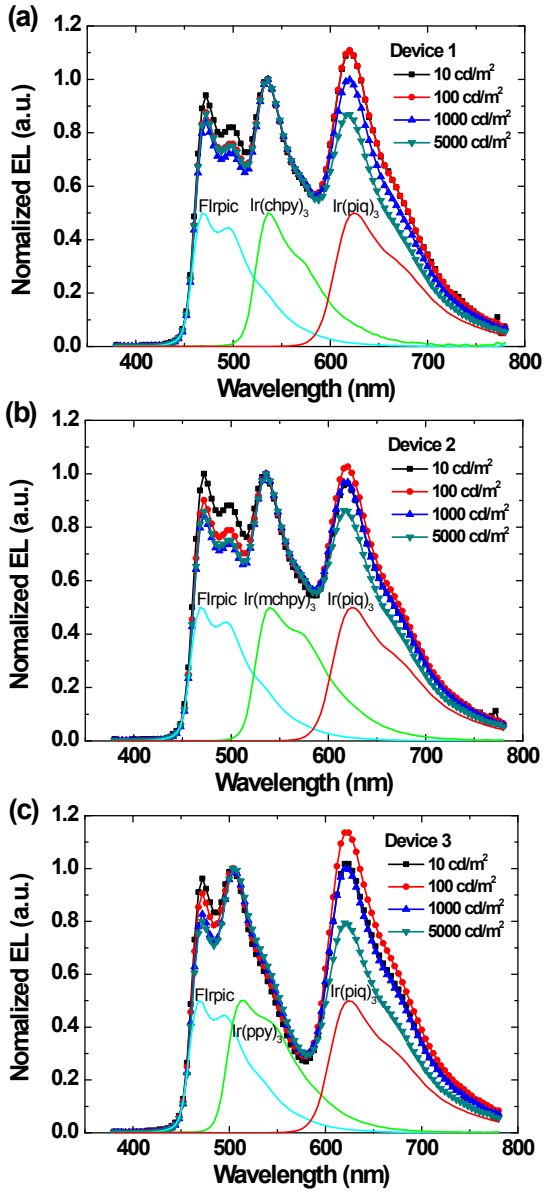

Figure 2.2 EL spectra of (a) device 1, (b) device 2, and (c) device 3 with different luminance. Solid lines are EL spectra of OLEDs with single emitting layer.

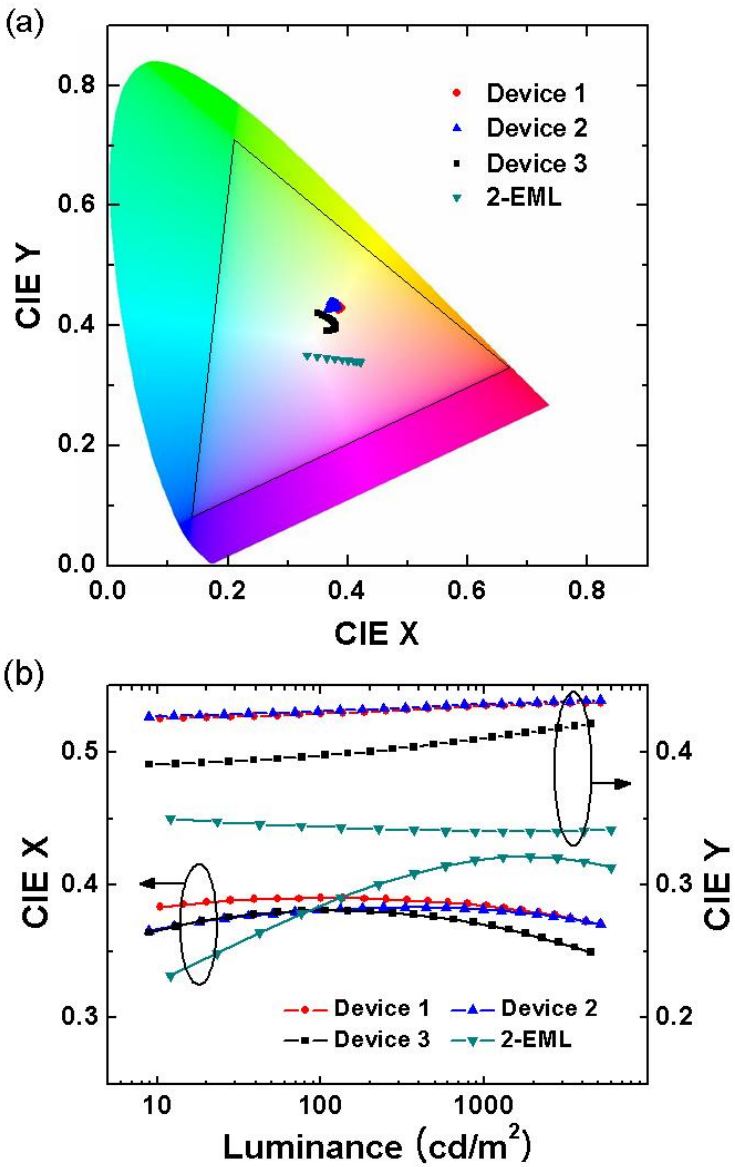

Figure 2.3 (a) CIE chromaticity coordinates of WOLEDs at luminance ranges of 10–5000 cd/m^2. (b) Variances of CIE X and CIE Y vs. luminance. Structure of 2-EML device is ITO / NPB (40 nm) / mCP:8%FIrpic (25 nm) / CBP:6%Ir(piq)$_3$ (5 nm) / BAlq (40 nm) / LiF (1 nm) / Al (100 nm).

depicted in Figure 2.1a, $Ir(chpy)_3$ [$Ir(mchpy)_3$] has the HOMO level of -5.0 eV (-5.1 eV) which is 1.1 eV (1.0 eV) higher than that of CBP, and the LUMO level of -2.5 eV (-2.6 eV) which is 0.4 eV (0.3 eV) higher than that of CBP. Due to the high HOMO levels of the dopants, the dopants act as deep traps of holes. At deep traps, detrapping probability of trapped charges is low and mobility of charge carrier is lowered. On the other hand, the LUMO levels of the dopants are higher than that of the host, so that electrons are scattered at the dopants sites. Then the mean free path of electrons is shortened and the drift velocity of the electrons gets lowered. Mobility of both charge carriers are reduced at the green EML. The reduction of the electron mobility by the doping is supported by the current density–voltage characteristics of the electron only devices where the current density of the device with the $Ir(chpy)_3$ doped CBP layer is lower than the CBP only or $Ir(ppy)_3$ doped CBP layers (Fig. 2.4). The reduced electron and hole mobilities by the dopants in the middle green emitting layer somehow lead to the recombination ratio in each layer constant with increasing current. On the contrary, $Ir(ppy)_3$ in CBP host works as a relatively shallower hole trap and doesn't function as an electron scattering center effectively because of the same LUMO level with the host as demonstrated in the Figure 2.4. Therefore, the recombination zone of the device 3 shifted more than the device 1 or 2.

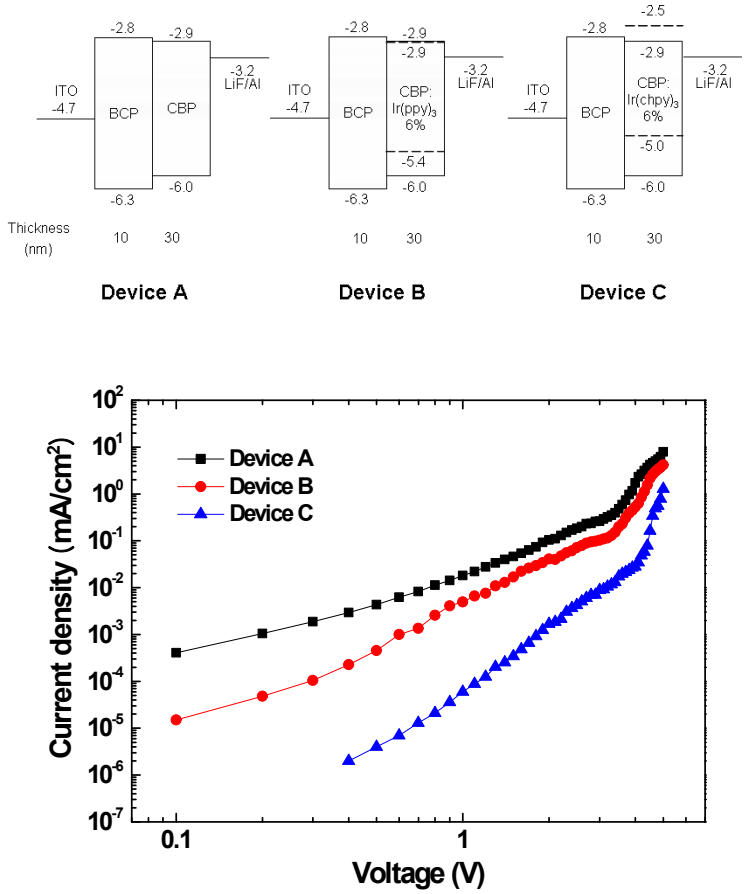

Figure 2.4 (a) Structures with energy levels and (b) current density-voltage characteristics of electron only devices.

This interpretation is further supported by a two-EML device [(ITO / NPB (40 nm) / mCP:8%FIrpic (25 nm) / CBP:6%Ir(piq)$_3$ (5 nm) / BAlq (40 nm) / LiF (1 nm) / Al (100 nm)] where the middle green EML layer was removed from the device 1 and 2. Spectral shift of the 2-EML devices are displayed in Figure 2.5. The two-EML device exhibited large shift of color coordinate as shown in Figure 2.3. This fact clearly demonstrates that the middle layer functions as the controlling layer preventing the recombination zone shift as well as the yellowish-green EML.

Figure 2.6a shows the current density–voltage–luminance characteristics of the WOLEDs. The luminance was measured for forwarded light from the devices. The turn-on voltages of the devices (1 cd/m^2) were 4.6, 4.5, and 4.7V for the device 1, 2, and 3, respectively. The turn-on voltages are almost the same as normal single layer phosphorescent OLEDs with the same hole and electron transporting layers. Maximum luminance of 50870 and 52600 cd/m^2 were obtained from the device 1 and 2 respectively, which are higher than 41560 cd/m^2 for the device 3.

External quantum efficiency and luminance efficiency of the emitted light in the forward direction of the WOLEDs versus current density are plotted in Figure 2.6b. Since the color coordinate of the device 1 and 2 were maintained almost constant for the whole range of the current density, the luminance

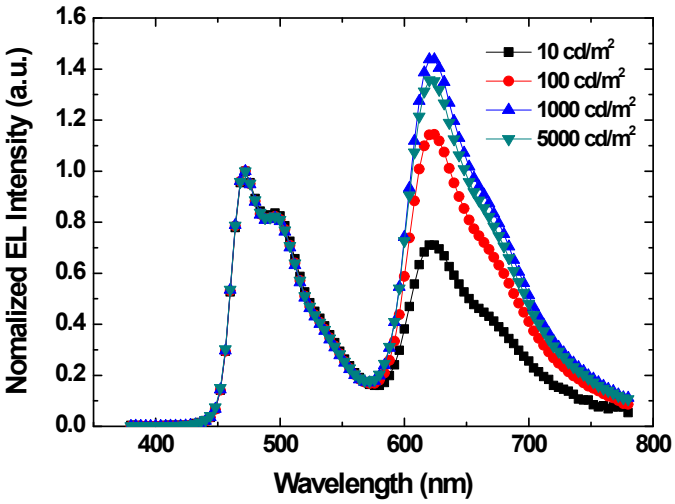

Figure 2.5 EL spectra of the 2-EML WOLED with the device structure of ITO / NPB (40 nm) / mCP:8%FIrpic (25 nm) / CBP:6%Ir(piq)$_3$ (5 nm) / BAlq (40 nm) / LiF (1 nm) / Al (100 nm).

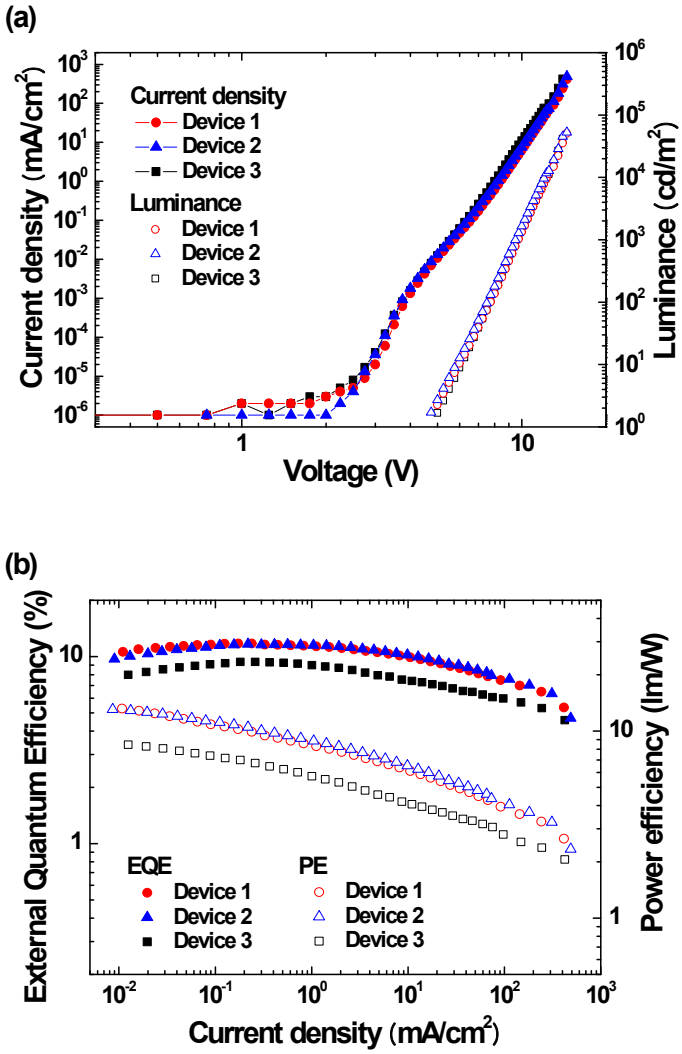

Figure 2.6 (a) Current density–voltage–luminance characteristic of the WOLEDs. (b) External quantum efficiency and power efficiency of the WOLEDs.

efficiency follows the same behavior as the external quantum efficiency. The external quantum efficiency and luminance efficiency of the device 1 (device 2) were 11.6% (11.6%) and 22.6 cd/A (23.3 cd/A) at 100 cd/m^2, 10.5% (10.8%) and 21.4 cd/A (22.3 cd/A) at 1,000 cd/m^2, and 8.9% (9.1%) and 18.8 cd/A (19.5 cd/A) at 5,000 cd/m^2, respectively. The maximum quantum efficiency and luminance efficiency of the WOLEDs were 11.7% and 22.8 cd/A for the device 1, and 11.7% and 23.4 cd/A for the device 2 at the current density of 0.2 mA/cm^2, respectively. The efficiency of these devices are higher than that of the device 3 (maximum quantum efficiency of 9.3% and maximum luminance efficiency of 15.0 cd/A). It implies that the balance between electrons and holes are improved by using the dopants having high energy levels. Moreover the external quantum efficiency of these WOLEDs remained high of 8.1% in the device 1 and 8.5% in the device 2 at luminance of 10000 cd/m^2 and the current density about 50 mA/cm^2. This low roll-off of efficiency is remarkable in phosphorescent WOLEDs. The efficiency of these devices are one of the highest values reported up to now. Maximum power efficiencies were 13.2 lm/W for the device 1 and 13.0 lm/W for the device 2, respectively, which are also much higher than 8.4 lm/W for the device 3. The power efficiency at 1000 cd/m^2 was dropped to 6.9 lm/W for the device 1 and 7.4 lm/W for the device 2, respectively. The low power efficiency can be

improved significantly if we adopt the doped electron and hole transporting layers or by reducing the thickness of the consisting layers.

2.4 Conclusion

In summary, efficient and color stable multi-EML phosphorescent WOLEDs had been presented using newly synthesized $Ir(chpy)_3$ and $Ir(mchpy)_3$ as yellowish-green dopants. The WOLEDs exhibited maximum external quantum efficiency of 11.7% and maximum luminance efficiency of 23.4 cd/A, and maximum power efficiency of 13.2 lm/W, respectively. The roll-off of efficiency was low with external quantum efficiency of 8.5% at 10000 cd/m^2 (~50 mA/cm^2). The WOLEDs also exhibited high CRI over 87 and the color temperature of about 4300 K. Moreover the WOLEDs showed very high color stability (CIE X = 0.37–0.38 and CIE Y = 0.43–0.44 at the luminance ranges of 10–5000 cd/m^2). The dopants have higher LUMO and HOMO levels than the host so that the dopants behave as hole traps and electron scattering centers. As a result the recombination ratio in each EML was maintained constant with increasing voltage to keep the CIE almost constant. The middle green emitting layer also improves the electron and hole balance in the EMLs to improve the device efficiency. According to these

characteristics, these WOLEDs have sufficient potential for solid-state lighting applications.

2.5 Bibliography

28. R. Duggal, J. J. Shiang, C. M. Heller, D. F. Foust, *Appl. Phys. Lett.* **2002**, 80, 3470.
29. J. Kido, K. Hongawa, K. Okuyama, K. Nagai, *Appl. Phys. Lett.* **1994**, 64, 815.
30. W. D'Andrade, R. J. Holmes, S. R. Forrest, *Adv. Mater.* **2004**, 16, 624.
31. C. H. Chuen, Y. T. Tao, *Appl. Phys. Lett.* **2002**, 81, 4499.
32. Y. Shao, Y. Yang, *Appl. Phys. Lett.* **2005**, 86, 073510.
33. J.-H. Jou, Y.-S. Chiu, C.-P.Wang, R.-Y.Wang, H.-C. Hu, *Appl. Phys. Lett.* **2006**, 88, 193501.
34. S. Kim, J. Seo, H. K. Jung, J.-J. Kim, S. Y. Park, *Adv. Mater.* **2005**, 17, 2077
35. Y.-H. Niu,M. S. Liu, J.-W. Ka, J. Bardeker, M. T. Zin, R. Schofield, Y. Chi, A. K.-Y. Jen, *Adv. Mater.* **2007**, 19, 300.
36. G. Tu, C. Mei, Q. Zhou, Y. Cheng, Y. Geng, L. Wang, D. Ma, X. Jing, F. Wang, *Adv. Funct. Mater.* **2006**, 16, 101.
37. J. Liu, Q. Zhou, Y. Cheng, Y. Geng, L.Wang,D.Ma, X. Jing, F. Wang, *Adv. Funct. Mater.* **2006**, 16, 957.
38. J. Jiang, Y. Xu, W. Yang, R. Guan, Z. Liu, H. Zhen, Y. Cao, *Adv. Mater.*

2006, 18, 1769.

39. V. Adamovich, J. Brooks, A. Tamayo, A. M. Alexander, P. I. Djurovich, B. W. D'Andrade, C. Adachi, S. R. Forrest, M. E. Thompson, *New J. Chem.* **2002**, 26, 1171.
40. J. Feng, F. Li,W. Gao, S. Liu, Y. Liu, Y. Wang, *Appl. Phys. Lett.* **2001**, 78, 3947.
41. B. W. D'Andrade, J. Brooks, V. Adamovich, M. E. Tompson, S. R. Forrest, *Adv. Mater.* **2002**, 14, 1032.
42. H. Kanno, R. J. Holmes, Y. Sun, S. Kena-Cohen, S. R. Forrest, *Adv. Mater.* **2006**, 18, 339.
43. F. Guo, D. Ma, *Appl. Phys. Lett.* **2005**, 87, 173510.
44. C.-C. Chang, J.-F. Chen, S.-W. Hwang, C. H. Chen, *Appl. Phys. Lett.* **2005**, 87, 253501.
45. T. Shiga, H. Fujikawa, Y. Taga, *J. Appl. Phys.* **2003**, 93, 19.
46. B. C. Krummacher, V.-E. Choong, M. K. Mathai, S. A. Choulis, F. So, F. Jermann, T. Fiedler, M. Zachau, *Appl. Phys. Lett.* **2006**, 88, 113506.
47. Y. Sun, N. C. Giebink, H. Kanno, B. Ma, M. E. Thompson, S. R. Forrest, *Nature* **2006**, 440, 908.
48. Y. Z. Wang, R. G. Sun, F. Meghdadi, G. Leising, A. J. Epstein, *Appl. Phys. Lett.* **1999**, 74, 3613.

49. C.-H. Kim, J. Shinar, *Appl. Phys. Lett.* **2002**, 80, 2201.

50. K. O. Cheon, J. Shinar, *Appl. Phys. Lett.* **2002**, 81, 1738.

51. G. Lei, L. Wang, Y. Qiu, *Appl. Phys. Lett.* **2006**, 88, 103508.

52. X.-M. Yu, H.-S. Kwok, W.-Y. Wong, G.-J. Zhou, *Chem. Mater.* **2006**, 18, 5097.

53. S. Lamansky, P. Djurovich,D.Murphy, F. Abdel-Razzaq, R. Keong, I. Tsyba, M. Bortz, B.Mui, R. Bau, M. E. Thompson, *Inorg. Chem.* **2001**, 40, 1704.

54. A. B. Tamayo, B. D. Alleyne, P. I. Djurovich, S. Lamansky, I. Tsyba, N. N. Ho, R. Bau, M. E. Thompson, *J. Am. Chem. Soc.* **2003**, 125, 7377.

55. D. M. Kang, J.-W. Kang, S. O. Jung, J. W. Park, S.-H. Lee, H.-D. Park, Y.-H. Kim, S. C. Shin, J.-J. Kim, S.-K. Kwon, *Adv. Mater.* **2008**, 20, 2003.

Chapter 3. Energy transfer from exciplexes to dopants and its effect on efficiency of organic light-emitting diodes

3.1 Introduction

Organic light-emitting diodes (OLEDs) have been successfully employed as small size displays and under active research for large size and flexible displays and solid state lighting. Reduction of the driving voltage is still an important issue, especially for solid state lighting in order to reduce power consumption. For this purpose, a few electron injection and transporting materials have been recently reported which posses low lowest unoccupied molecular orbital (LUMO) energy levels below –3.0 eV for efficient electron injection from a cathode to the electron transporting layer (ETL) by lowering the electron injection barrier.[1,2] However, these ETLs have a potential to form exciplexes at the interface between the emitting layer (EML) host and the ETL because of the large energy difference of the LUMO and highest occupied molecular orbital (HOMO) energy levels between the EML host and the ETL, leading to a charge transfer from the EML host (donor) to the ETL

(acceptor) to form a charge transfer complex (exciplex). The formation of an exciplex usually leads to a red-shifted emission and broadened spectrum relative to the emissions of the individual acceptor or donor.[3] Also, the exciplex formation generally leads to a low electroluminescence (EL) efficiency of the OLEDs.[4] Although there has been some research on the application of the exciplex formation to the tuning of emission colors[5–10] or to white OLEDs,[11–14] the formation of an exciplex is an obstacle for high-efficiency OLEDs. A few methods for eliminating the exciplex emission have been reported. They include the use of a hole transporting layer (HTL) or an ETL which has a low energy barrier with the EML[3,6,15–17] or the insertion of an exciplex-preventing layer at the donor/acceptor interface.[18–21] Most previous studies about exciplexes in the OLEDs have dealt with the reduction of the exciplex formation to enhance the efficiency of the OLEDs.

In this study, we report that exciplexes are indeed formed at the interface between a widely used EML host material, N,N'-dicarbazolyl-4-4'-biphenyl (CBP) and a recently reported high performance ETL material, bis-4,6-(3,5-di-3-pyridylphenyl)-2-methylpyrimidine (B3PYMPM). This exciplex formation can significantly reduce the efficiency of the OLEDs. However, the exciplexes formed at the EML/ETL interface were effectively harvested to produce light by the doping of the *fac*-tris(2-phenylpyridine) iridium

[$Ir(ppy)_3$] in the EML to exceed a 20% external quantum efficiency. The energy transfer processes were successfully analyzed by the Förster energy transfer mechanism. We also observed the change of the exciplex emission intensity and the efficiency roll-off of the OLEDs by the variation of the distance between the exciplex and the dopant.

3.2 Experimental

The OLEDs were fabricated by thermal evaporation onto cleaned glass substrates precoated with indium tin oxide (ITO) without breaking the vacuum. Prior to organic layer deposition, the ITO substrates were exposed to UV-ozone flux for 10 min following degreasing in acetone and isopropyl alcohol. All layers were grown by thermal evaporation at a base pressure of < 5×10^{-7} Torr. The layers were deposited in the following order: 1,1-bis-(4-bis(4-methyl-phenyl)-amino-phenyl)-cyclohexane (TAPC):8 wt. % ReO_3 (20 nm) / TAPC (30 nm) / EML / B3PYMPM (30 nm) / B3PYMPM: 15 wt. % Rb_2CO_3 (20 nm) / Al (100 nm). We fabricated two series of the OLEDs, which have different EML structures. The EMLs of the series 1 OLEDs are CBP: x mol. % $Ir(ppy)_3$ (15 nm) with x=1, 2, 3, 4, 5, and 6 mol. %, respectively. The EMLs of the series 2 OLEDs are CBP: 6 mol. % $Ir(ppy)_3$ (15 nm) / CBP (y

nm), with y=0, 1, 2, and 3 nm, respectively. The structure of the OLEDs and the energy level diagram of the materials used in this study are shown in Figure 3.1.

The highest occupied molecular orbital (HOMO) levels of the organic materials, except CBP and B3PYMPM, are obtained from the cyclic voltammetry measurement, while the LUMO levels are calculated from the HOMO level and the energy gap is obtained from the edge of the absorption spectra. The HOMO and the LUMO levels of the CBP and B3PYMPM are obtained from the published literature.[1,22]

Organic films for the photoluminescence (PL) spectrum and efficiency measurements were fabricated by the thermal evaporation on pre-cleaned quartz substrates at the base pressure of $< 5\times10^{-7}$ Torr. The PL spectra and the PL efficiency of the organic films were measured using an integrating sphere. A continuous wave He/Cd laser (325 nm) was used as the excitation light source, and a monochromator attached with a photomultiplier tube was used as the optical detector system. Low-temperature (low-T) PL spectra were measured in a cryostat cooled down to as low as 10 K using an intensified charge-coupled device (ICCD) with a pulsed Nd–YAG laser (355 nm) as the excitation light source.

The current density, luminance, and electroluminescence (EL) spectrum of the

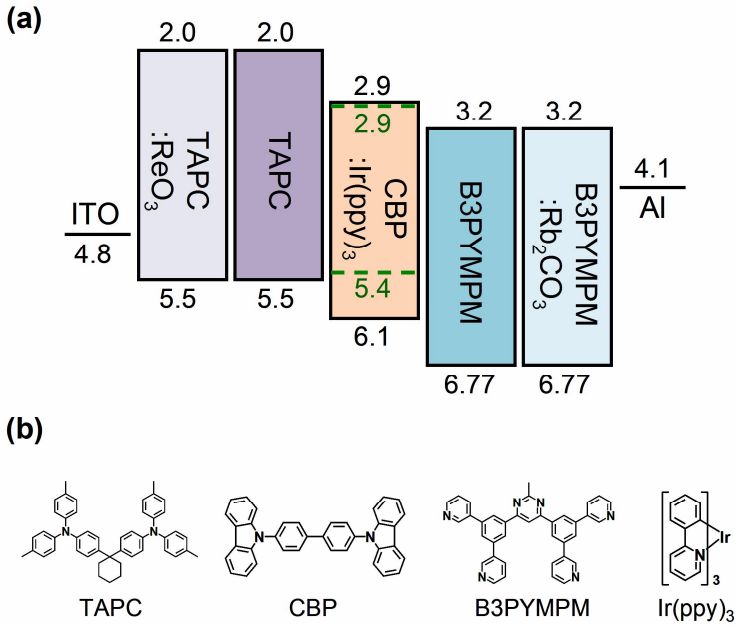

Figure 3.1 (a) Device structure of the OLEDs and energy levels of the materials. (EML of the series 1 OLEDs; CBP: x mol. % $Ir(ppy)_3$ (15 nm), EML of the series 2 OLEDs; CBP: 6 mol. % $Ir(ppy)_3$ (15 nm) / CBP (y nm)). (b) Molecular structure of the materials used in the study.

OLEDs were measured simultaneously using a Keithley 2400 programmable source meter and a SpectraScan PR650 (Photo Research). The external quantum efficiency (EQE) of the OLEDs was calculated from spectral luminance intensity in the forward direction of the OLEDs.

3.3 Result and Discussion

The PL spectra of CBP, B3PYMPM, and CBP:B3PYMPM co-deposited films were measured to identify the exciplex formation between the CBP and the B3PYMPM and are shown in Figure 3.2a. The molar ratio of the CBP to the B3PYMPM of the CBP:B3PYMPM co-deposited film is 1:1. The PL emission peaks of the CBP, B3PYMPM, and CBP:B3PYMPM films are located at 380 nm, 395 nm, and 425 nm, respectively. The PL emission peak of the CBP:B3PYMPM is red-shifted from the CBP or B3PYMPM, and the energy of the CBP:B3PYMPM emission peak is 2.9 eV. The energy level corresponds to the difference between the HOMO level of the CBP and the LUMO level of the B3PYMPM, proving that CBP and B3PYMPM molecules form the exciplexes upon excitation. In addition, the emission peaks of CBP and B3PYMPM do not appear in the PL spectrum of the CBP:B3PYMPM film, indicating that almost all the excitons in the CBP:B3PYMPM film form

the exciplexes. Therefore, this exciplex formation between CBP and the B3PYMPM can significantly reduce the emission efficiency of the OLEDs.

The low-T PL spectra of the CBP and the CBP:B3PYMPM co-deposited films were measured to verify the energy level of the triplet exciplex (Figure 3.2b). The low-T PL spectrum of the CBP film shows the phosphorescence emission peaks (485, 525, and 565 nm) in addition to the fluorescence emission peaks (380 and 400 nm). The low-T PL spectrum of the CBP:B3PYMPM film shows the phosphorescence emission of the CBP (485, 525, and 565 nm) and the fluorescence emission of the exciplex (425 nm), but the phosphorescence emission of the exciplex does not appear. Therefore, we cannot specify the energy level of the triplet exciplex from these data. However, it can be inferred that the energy level of the triplet exciplex is higher than the T_1 level of the CBP, because the CBP phosphorescence emission intensity of the CBP:B3PYMPM co-deposited film is higher than that of the CBP film. In such a case, the triplet exciplex is expected to transfer energy to the T_1 state of CBP rather than to the ground state, because the spin is conserved. Therefore, the phosphorescence emission of the exciplex does not appear and the CBP phosphorescence emission becomes stronger.

Figure 3.3a shows the normalized EL spectra of the series 1 OLEDs in a semi-log plot. The exciplex emission is observed in the EL spectra in addition to the

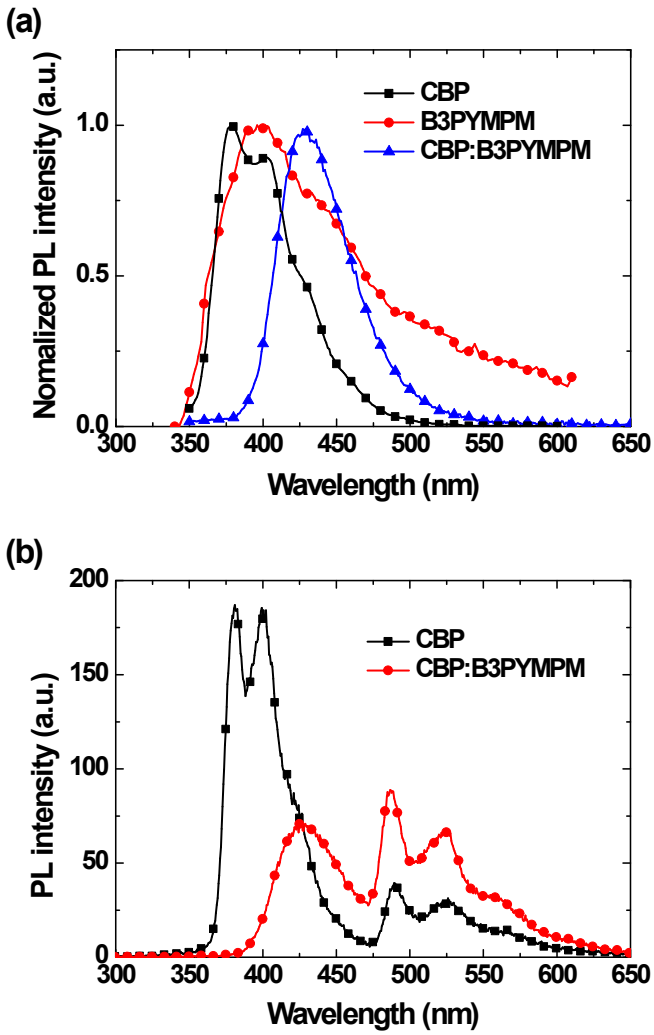

Figure 3.2 (a) Normalized PL spectra of CBP, B3PYMPM, and CBP:B3PYMPM co-deposited films. (b) Low-T PL spectra of CBP and CBP:B3PYMPM co-deposited films.

emission from the $Ir(ppy)_3$. The exciplex emission is decreased as the concentration of the $Ir(ppy)_3$ increases. The dependence of the exciplex emission on the dopant concentration can be understood based on the energy transfer of the singlet exciplex to the dopant. Since the emission spectrum of the singlet exciplex overlaps with the singlet absorption of the $Ir(ppy)_3$,[23] the energy of the singlet exciplex can be transferred to the $Ir(ppy)_3$. In such a case, the emission efficiency of the singlet exciplex can be expressed as

$$\Phi_{ex} = \frac{k_{ex,r}}{k_{ex,r} + k_{ex,nr} + k_{ex-dop}}, \quad (1)$$

where $k_{ex,r}$ is the radiative decay rate of the exciplex, $k_{ex,nr}$ is the non-radiative decay rate of the exciplex, and k_{ex-dop} is the energy transfer rate from the exciplex to the dopant. Assuming that the exciplex-dopant energy transfer takes place via the Förster energy transfer, then

$$k_{ex-dop} \propto {r_{ex-dop}}^{-6} \propto {c_{dop}}^{2}, \quad (2)$$

where r_{ex-dop} is the mean distance between the exciplex and the dopant and

c_{dop} is the concentration of the dopant.[24] If the decay rate of the exciplex is much slower than the exciplex dopant energy transfer rate ($k_{ex,r} + k_{ex,nr} << k_{ex-dop}$), then the emission efficiency of the exciplex is as follows:

$$\Phi_{ex} \cong \frac{k_{ex,r}}{k_{ex-dop}} \propto {c_{dop}}^{-2}. \quad (3)$$

This relationship predicts that the exciplex emission intensity is proportional to the inverse square of the dopant concentration if the energy transfer is the reason for the reduction of the exciplex emission. To confirm the energy transfer from the exciplex to the dopant, the intensity of the exciplex emission is plotted as a function of the $Ir(ppy)_3$ concentration in Figure 3.3b. The intensity of the exciplex emission is indeed approximately proportional to the inverse square of the $Ir(ppy)_3$ concentration, demonstrating that the reduction of the exciplex emission with an increase in the $Ir(ppy)_3$ concentration originates from the energy transfer from the exciplex to the $Ir(ppy)_3$.

The formation of the exciplex influences the EQE of the OLEDs, as shown in Figure 3.3c, where the EQE and the exciplex emission ratio of the series 1 OLEDs are plotted as a function of the current density. The exciplex emission

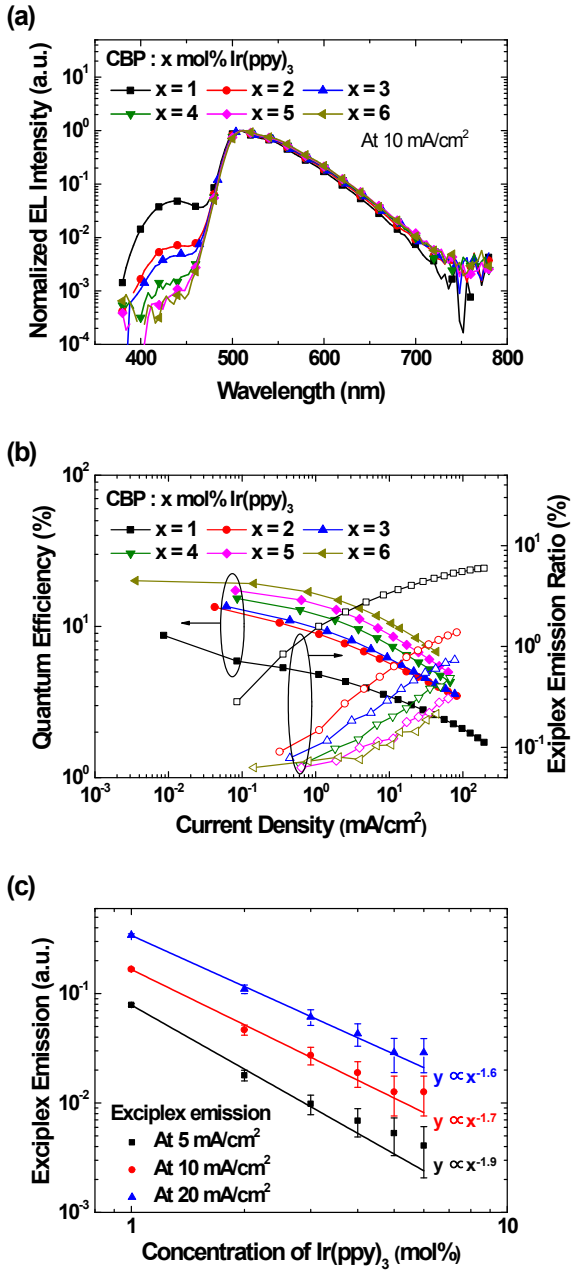

Figure 3.3 (a) Normalized EL spectra of the series 1 OLEDs. (b)Intensity of the exciplex emission as a function of the $Ir(ppy)_3$ concentration. (c) External quantum efficiency and exciplex emission ratio of the series 1 OLEDs.

ratio is defined as the ratio of the integrated number of emitted photons from the exciplex to the integrated total number of emitted photons. The exciplex emission ratio depends on the doping concentration of the $Ir(ppy)_3$ and the current density. The EQEs are inversely proportional to the exciplex emission ratio, and the maximum EQE reaches 20.1% when the doping concentration of $Ir(ppy)_3$ is 6 mol. % and the current density is low. However, this is not the only reason for the low efficiency of OLEDs with low $Ir(ppy)_3$ concentration. The Dexter transfer rate from the host to the dopant decreases as the concentration of the dopant decreases, and then the efficiency of the OLEDs also decreases.[25] However, it is hard to separate the efficiency reduction by the exciplexes and the efficiency reduction by the host-dopant energy transfer. The increase in the exciplex emission with the current density can be interpreted based on the shift of the emission zone in the EML toward the direction of the ETL as the current density increases, since the exciplex is formed at the EML/ETL interface.[26] The shift of the emission zone is supported by the reduction of the relative intensity of the long wavelength shoulder in the emission spectrum with the increasing driving voltage (Figure 3.4). This fact indicates that the excitons are formed near the HTL at low current densities and as current density increase, more electrons and holes recombine near the EML/ETL interface, leading to the formation of more

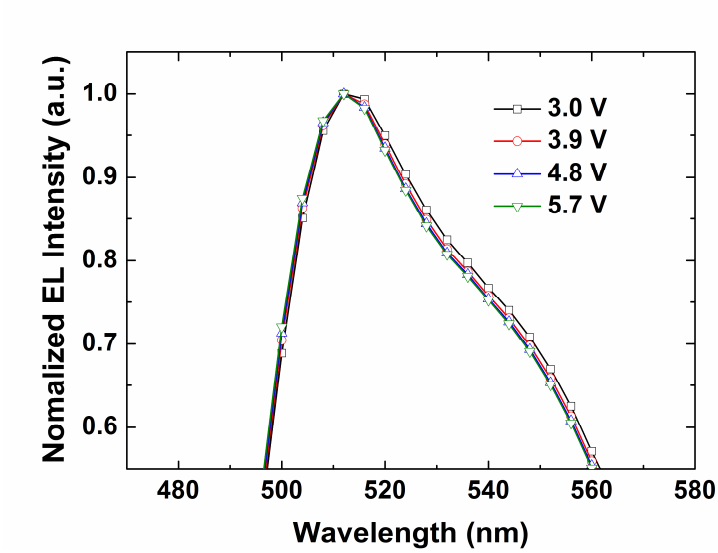

Figure 3.4 Enlarged graph of normalized EL spectra of the series 1 OLED with 6 mol% $Ir(ppy)_3$ concentration at different driving voltage.

exciplexes.

Up to now, we have limited our discussion to the singlet exciplex. The triplet exciplex may be transferred to the CBP via a Dexter energy transfer mechanism followed by an energy transfer to the $Ir(ppy)_3$, because the T_1 state of the CBP is smaller than the energy gap of the triplet exciplex. The energy transfer rate from the triplet exciplex to the CBP should not be influenced by the doping concentration of the $Ir(ppy)_3$. Figure 3.5 shows a schematic diagram of the energy transfer processes at the EML/ETL interface of the OLEDs.

The increase in the exciplex emission will affect the efficiency roll-off of the OLEDs. To investigate the relationship between the efficiency roll-off of the OLEDs and the energy transfer from the exciplexes to dopants, we inserted a thin, undoped CBP layer at the EML/ETL interface, keeping the concentration of the $Ir(ppy)_3$ in the EML constant (series 2 OLEDs). The distance between the exciplex and the dopant is controlled by the variation of the undoped CBP layer thickness. Figure 3.6a shows the normalized EL spectra of the series 2 OLEDs as semi-log plots. The exciplex emission increases as the thickness of the undoped CBP layer increases, which is expected due to the reduced energy transfer rate from the exciplexes to the dopants with the increasing distance between the exciplexes and the dopants. Figure 3.6b shows the EQE and the

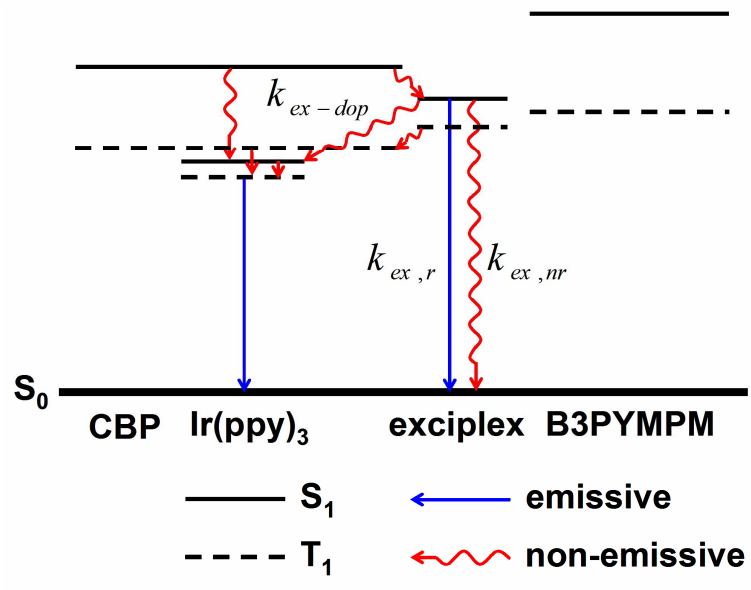

Figure 3.5 Schematic diagram of the energy transfer at the EML/ETL interface of the OLEDs.

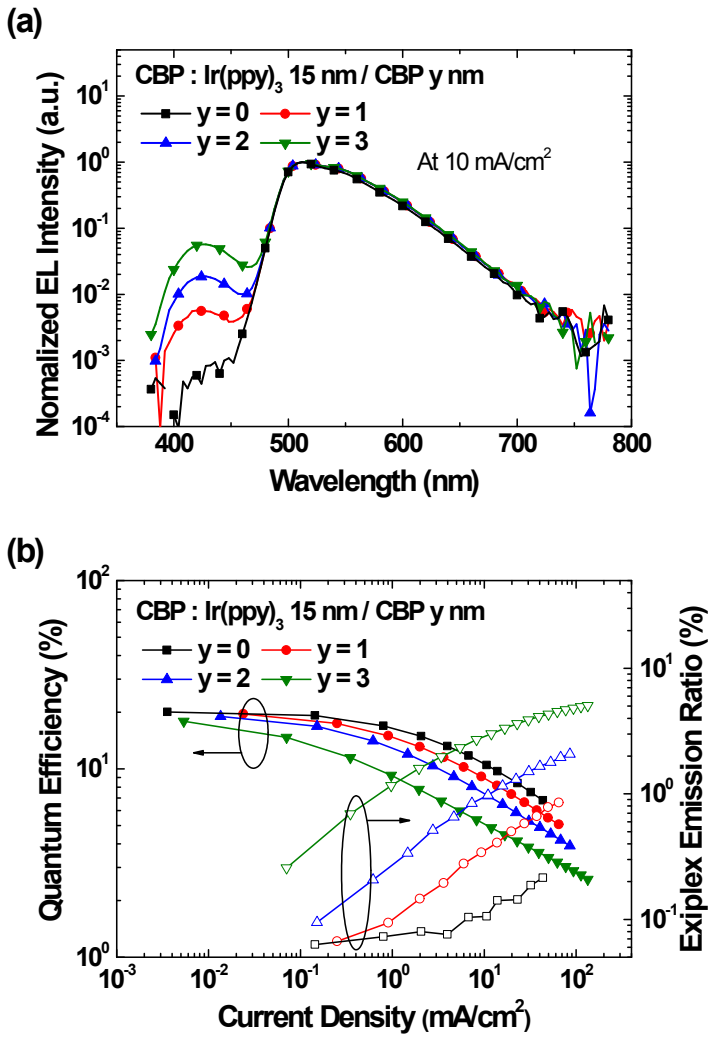

Figure 3.6 (a) Normalized EL spectra of the series 2 OLEDs. (b) External quantum efficiency and exciplex emission ratio of the series 2 OLEDs.

exciplex emission ratio of the series 2 OLEDs as a function of the current density. The exciplex emission ratio is low and the EQE values of all devices are similar at low current density. As the current density increases, both the exciplex emission ratio and the efficiency roll-off increase. The OLED with a thicker undoped CBP layer shows a larger exciplex emission ratio and efficiency roll-off. It can be interpreted that the exciplex emission is the reason for this difference in the efficiency roll-off among the OLEDs.

The reduction in the efficiency by the formation of exciplexes was calculated. If all the triplet exciplexes are transferred to the $Ir(ppy)_3$ via the CBP, the EQE of the OLEDs can be expressed as follows:

$$\eta_{ext} = \eta_{re}\eta_{out}\left[\left(1 - R_{ex} + \frac{3}{4}R_{ex}\right)\eta_{PL,Ir(ppy)_3} + \frac{1}{4}R_{ex}\eta_{PL,ex}\right]\eta_{EL}(J), \quad (4)$$

where η_{re} is the recombination efficiency of the hole and electron, η_{out} is the outcoupling efficiency, R_{ex} is the exciplex formation ratio, $\eta_{PL,Ir(ppy)_3}$ and $\eta_{PL,ex}$ are the PL efficiencies of the $Ir(ppy)_3$ and the exciplex, respectively, and $\eta_{EL}(J)$ is the current density–dependent EL efficiency considering the efficiency reduction mechanisms of the triplet-triplet annihilation (TTA) or exciton-polaron quenching. Assuming all of the charges

are recombined and the PL efficiency of the $Ir(ppy)_3$ is 100%,[27] the EQE can be expressed as follows:

$$\eta_{ext} = \left(1 - \frac{1}{4}R_{ex} + \frac{1}{4}R_{ex}\eta_{PL,ex}\right)\eta_{out}\eta_{EL}(J). \quad (5)$$

Therefore, the reduction of the EQE by the exciplexes ($\eta_{r,ex}$) can be expressed as follows:

$$\eta_{r,ex} = \frac{1}{4}R_{ex}\left(1 - \eta_{PL,ex}\right)\eta_{out}\eta_{EL}(J). \quad (6)$$

The exciplex formation ratio can be obtained from the exciplex emission ratio (r_{ex}). The exciplex contributing portion of the EQE can be expressed as follows:

$$\eta_{ext}r_{ex} = \frac{1}{4}R_{ex}\eta_{PL,ex}\eta_{out}\eta_{EL}(J) \quad (7)$$

$$R_{ex} = \frac{4\eta_{ext}r_{ex}}{\eta_{PL,ex}\eta_{out}\eta_{EL}(J)}. \quad (8)$$

Therefore, the reduction of the EQE by the exciplexes is calculated by the

following equation:

$$\eta_{r,ex} = \eta_{ext} r_{ex} \left(\frac{1}{\eta_{PL,ex}} - 1 \right) \tag{9}$$

The PL efficiency of the exciplex is 0.11, which is obtained from the CBP:B3PYMPM (1:1) film. Figure 3.7 shows the calculated reduction of the EQE by the exciplex of the series 2 OLEDs. The difference between the calculated efficiency reduction by the exciplex between the OLED without the undoped CBP layer and the OLED with a 3-nm-thick undoped CBP layer is 1.1% at 30 mA/cm^2. It is smaller than the difference of the EQE between the two OLEDs (3.8% at 30 mA/cm^2). We speculate that this difference between the calculated value and the experimental data occurs because the triplet exciplexes are not transferred to the $Ir(ppy)_3$ efficiently, due to the undoped CBP layer. We calculate the reduction in the efficiency due to the exciplexes, again assuming that the triplet exciplexes are not transferred to the $Ir(ppy)_3$. The EQE of the OLEDs and the reduction of the EQE by the exciplexes can then be expressed as follows:

$$\eta_{ext} = \left(1 - R_{ex} + \frac{1}{4} R_{ex} \eta_{PL,ex}\right) \eta_{out} \eta_{EL}(J), \tag{10}$$

$$\eta_{r,ex} = \eta_{ext} r_{ex} \left(\frac{4}{\eta_{PL,ex}} - 1\right). \tag{11}$$

The calculated reduction of the EQE by the exciplex, assuming that no triplet exciplexes are transferred to the $Ir(ppy)_3$, is also shown in Fig. 3.7. In this case, the difference between the calculated efficiency reduction by the exciplex between the OLED without the undoped CBP layer and the OLED with a 3-nm-thick undoped CBP layer is 4.8% at 30 mA/cm^2. It is larger than the difference in the EQEs between the two OLEDs. These two calculation results indicate that the triplet exciplexes are partially transferred to the $Ir(ppy)_3$ via the CBP. Delayed fluorescence of the exciplex due to the TTA at the CBP/B3PYMPM interface can be one of the reasons for the difference between the calculated value and the experimental data. However, more research is needed to quantify the effect of the delayed fluorescence of the exciplex by the TTA.

3.4 Conclusion

We investigated the production of high-efficiency OLEDs through the energy

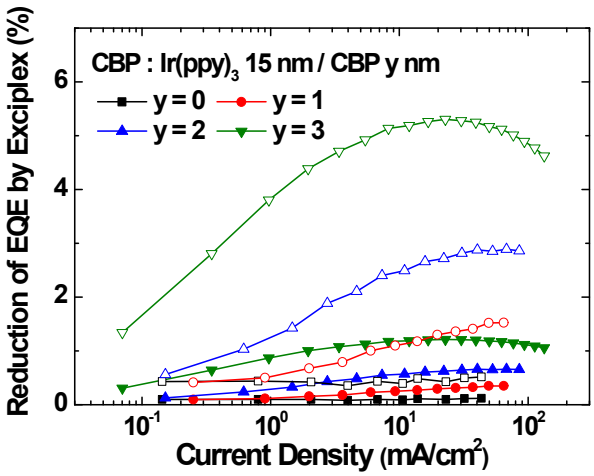

Figure 3.7 Calculated reduction of the EQE by the exciplex of the series 2 OLEDs, assuming the triplet exciplexes are transferred to the $Ir(ppy)_3$ (closed symbols) and assuming the triplet exciplexes are not transferred to the $Ir(ppy)_3$ (open symbols).

transfer process from the exciplexes to the dopants. The CBP and the B3PYMPM form exciplexes due to excitations at the EML/ETL interface of the OLEDs. This exciplex formation can significantly reduce the efficiency of the OLEDs. However, the energy of the exciplex is transferred to the $Ir(ppy)_3$, and it reduces the efficiency reduction by the exciplexes. The energy transfer processes were successfully analyzed by the Förster energy transfer mechanism. The energy transfer rate from the exciplexes to the $Ir(ppy)_3$ increases as the distance between the exciplexes and the $Ir(ppy)_3$ decreases. Therefore, the efficiency of the OLEDs is enhanced as the concentration of the $Ir(ppy)_3$ increases. The maximum EQE reached 20.1% in the OLED when it was doped with 6 mol. % $Ir(ppy)_3$.

Also, the exciplex emission ratio of the OLEDs increases as the current density increases, leading to the additional roll-off of efficiency in the OLEDs at high current. The relationship between the efficiency roll-off of the OLEDs and the energy transfer from the exciplexes to the dopants was analyzed by inserting a thin, undoped CBP layer at the EML/ETL interface.

3.5 Bibliography

1. D. Tanaka, H. Sasabe, Y.-J. Li, S.-J. Su, T. Takeda, and J. Kido, *Jpn. J. Appl. Phys.* **2007**, 46, L10.
2. D. Tanaka, Y. Agata, T. Takeda, S. Watanabe, and J. Kido, *Jpn. J. Appl. Phys.* **2007**, 46, L117.
3. W. M. Su, W. L. Li, Q. Xin, Z. S. Su, B. Chu, D. F. Bi, H. He, and J. H. Niu, *Appl. Phys. Lett.* **2007**, 91, 043508.
4. N. Matsumoto, M. Nishiyama, and C. Adachi, *J. Phys. Chem. C* **2008**, 112, 7735.
5. J. A. Osaheni and S. A. Jenekhe, *Macromolecules* **1994**, 27, 739.
6. K. Itano, H. Ogawa, and Y. Shirota, *Appl. Phys. Lett.* **1998**, 72, 636.
7. K. Okumoto and Y. J. Shirota, *J. Lumin.* **2000**, 87–89, 1171.
8. G. Cheng, Y. Zhang, Y. Zhao, S. Liu, Z. Xie, H. Xia, M. Hanif, and Y. Mab, *Appl. Phys. Lett.* **2005**, 87, 013506.
9. M. Li, W. Li, L. Chen, Z. Kong, B. Chu, B. Li, Z. Hu, and Z. Zhang, *Appl. Phys. Lett.* **2006**, 88, 091108.
10. C. J. Liang and W. C. H. Choy, *Appl. Phys. Lett.* **2007**, 89, 251108.
11. J. Feng, F. Li, W. Gao, S. Liu, Y. Liu, and Y. Wang, *Appl. Phys. Lett.* **2001**, 78, 3947.

12. Q. J. Sun, B. H. Fan, Z. A. Tan, C. H. Yang, Y. F. Li, and Y. Yang, *Appl. Phys. Lett.* **2006**, 88, 163510.

13. Q.-X. Tong, S.-L. Lai, M.-Y. Chan, J.-X. Tang, and H.-L. Kwong, *Appl. Phys. Lett.* **2007**, 91, 023503.

14. J. Kalinowski, M. Cocchi, D. Virgili, V. Fattori, and J. A. G. Williams, *Adv. Mater.* **2007**, 19, 4000.

15. N. Tamoto, C. Adachi, and K. Nagai, *Chem. Mater.* **1997**, 9, 1077.

16. C. Giebeler, H. Antoniadis, D. D. C. Bradley, and Y. Shirota, *J. Appl. Phys.* **1999**, 85, 608.

17. M. Castellani and D. Berner, *J. Appl. Phys.* **2007**, 102, 024509.

18. G. Li, C. H. Kim, Z. Zhou, J. Shinar, K. Okumoto, and Y. Shirota, *Appl. Phys. Lett.* **2006**, 88, 253505.

19. G. He, M. Pfeiffer, M. Hofmann, J. Birnstock, R. Pudzich, J. Salbeck, and K. Leo, *Appl. Phys. Lett.* **2004**, 85, 3911.

20. S.-H. Liao, J.-R. Shiu, S.-W. Liu, S.-J. Yeh, Y.-H. Chen, C.-T. Chen, T. J. Chow, and C.-I. Wu, *J. Am. Chem. Soc.* **2009**, 131, 763.

21. T. Noda, H. Ogawa, and Y. Shirota, *Adv. Mater.* **1999**, 11, 283.

22. V. I. Adamovich, S. R. Cordero, P. I. Djurovich, A. Tamayo, M. E. Thompson, B. W. D'Andrade, and S. R. Forrest, *Org. Electron.* **2003**, 4, 77.

23. T. Tsuboia and M. Tanigawa, *Thin Solid Films*, **2003**, 438–439, 301.

24. T. Förster, *Discuss. Faraday Soc.* **1959**, 27, 7.

25. M. A. Baldo, S. Lamansky, P. E. Burrows, M. E. Thompson, and S. R. Forrest, *Appl. Phys. Lett.* **1999**, 75, 4.

26. J.-W. Kang, S.-H. Lee, H.-D. Park, W.-I. Jeong, K.-M. Yoo, Y.-S. Park, and J.-J. Kim, *Appl. Phys. Lett.* **2007**, 90, 223508.

27. S.-Y. Kim and J.-J. Kim, *Org. Electron.* **2010**, 11, 1010.

Chapter 4. Efficient Triplet Harvesting by Fluorescent Molecules through Exciplexes for High Efficiency Organic Light-Emitting Diodes

4.1 Introduction

The internal quantum efficiency (IQE) of fluorescent organic light-emitting diodes (OLEDs) is limited to 25% because only singlet excitons are used for light emission. On the other hand, phosphorescent OLEDs can achieve a 100% IQE because both the singlet and the triplet excitons can be harvested to produce light. However, phosphorescent materials suffer from instability for practical applications, especially for the color blue.[1] There are still a lot of efforts to synthesize stable and efficient blue phosphorescent materials.[2,3] An alternative way to overcome the instability problem of phosphorescent materials is to use delayed fluorescence, by converting the triplet exciton to a singlet exciton. Primarily two methods have been exploited for this purpose up to now: triplet-triplet annihilation (TTA),[4-6] and thermally activated delayed fluorescence (TADF).[7-9]

TTA is the process in which one singlet exciton and one ground state is

produced by the collision of two triplet excitons. It is a mechanism which reduces the efficiency in phosphorescent OLEDs, but the production of the singlet excitons by the TTA can enhance the electroluminescence (EL) efficiency in fluorescent OLEDs. This additional singlet exciton production can increase the internal EL efficiency significantly, even though the TTA process is much more complicated than just the formation of a singlet exciton.[10]

The TADF is a recently proposed mechanism to convert the trip-let excitons into the singlet excitons by thermal activation. There-fore, a small energy difference between the singlet and the triplet excited states ($\Delta E_{1\text{-}3}$) is required for efficient TADF. A small $\Delta E_{1\text{-}3}$ value can be achieved when the overlap between the highest occupied molecular orbital (HOMO) and the lowest unoccupied molecular orbital (LUMO) of a molecule is small. Molecules com-posed of electron donor and acceptor groups are demonstrated to have small $\Delta E_{1\text{-}3}$.[7,8]

An exciplex is an excited charge-transfer complex formed by an electron donor molecule and an electron acceptor molecule. In other words, the exciplex is a kind of intermolecular donor-acceptor system. Therefore, the exciplex has the potential to have a small positive or negative $\Delta E_{1\text{-}3}$ value,[11,12] enabling efficient reverse inter-system crossing (RISC) from the triplet

charge-transfer (CT) states to the singlet CT states. The emission spectrum of the exciplex is usually broad and red-shifted relative to the emissions of the individual acceptor or donor,[13] and the emission efficiency of the exciplex is generally low.[14] Although there has been some research on the application of the exciplex to the tuning of the emission colors[15-20] or to white OLEDs,[21-24] the formation of the exciplex is considered to be an obstacle for high-efficiency OLEDs. Moreover, there are few reports on the utilization of exciplexes to harvest triplet excited states for EL. Recently, RISC from the triplet exciplex to the singlet exciplex was reported. The OLEDs fabricated using the material systems showed the external quantum efficiency (EQE) as high as 5.4%.[25]

In this work, we report not only the efficient harvesting of triplet excited states from exciplexes using a different exciplex forming material system composed of a hole transporting material, 4,4',4''-tris(N-carbazolyl)-triphenylamine (TCTA), and an electron trans-porting material, bis-4,6-(3,5-di-3-pyridylphenyl)-2-methylpyrimidine (B3PYMPM) (Figure 4.1a), but also report that almost 100% PL efficiency is obtained from the exciplexes at low temperature (low-T). Moreover the EQE of the OLED using the material system increased to 10% from 3.1% as the temperature goes down to 195 K from room temperature (RT), which is much higher than the limitation of the

singlet exciplex. Also, energetics of the singlet and triplet exciplex is discussed to understand the behavior.

4.2 Experimental

The OLEDs were fabricated by thermal evaporation onto cleaned glass substrates precoated with 150 nm-thick indium tin oxide (ITO). Prior to organic layer deposition, the ITO substrates were exposed to UV-ozone flux for 10 min following degreasing in acetone and isoprophylalcohol. All layers were grown by thermal evaporation at a base pressure of $< 5\times10^{-7}$ Torr without breaking the vacuum. The layers were deposited in the following order: 1,1-bis-(4-bis(4-methyl-phenyl)-amino-phenyl)-cyclohexane (TAPC) (30 nm) / TCTA (10 nm) / TCTA:B3PYMPM (30 nm) / B3PYMPM (20~40 nm) / LiF (1 nm) / Al (100 nm) (Figure 4.1b). The molar ratio of the TCTA to the B3PYMPM of the co-deposited TCTA:B3PYMPM layer is 1:1. The HOMO and the LUMO levels of the organic materials are obtained from the published literature.[26-28] The EQE of the OLED was calculated from the current density, luminance, and EL spectra data which were measured using a Keithley 2400 programmable source meter and a SpectraScan PR650 (Photo Research). Transient EL of the OLEDs was measured by an Agilent 8114A

pulse generator combined with a monochromator attached photomultiplier tube (PMT). The excitation pulse width was 100 μs and the baseline voltage was -1 V.

The organic films for the measurement of the PL spectra, time resolved PL spectra and transient PL measurements were fabricated by thermal evaporation on precleaned quartz substrates at a base pressure of $< 5\times10^{-7}$ Torr. At room temperature (RT), the PL spectra and the PL efficiency of the organic films were measured using an integrating sphere.[29] A continuous wave He/Cd laser (325 nm) was used as the excitation light source and the monochromator attached PMT as the optical detector system. The time resolved PL spectra, the transient PL, and the low-temperature PL efficiency were measured in a cryostat, and the organic films were cooled down from 300 K to 35 K. A pulsed Nd–YAG laser (355 nm) was used as the excitation light source and an intensified charge-coupled device (ICCD) was used as the optical detector for the measurement.

4.3 Result and Discussion

Figure 4.1c shows the PL spectra of the TCTA, the B3PYMPM and the TCTA:B3PYMPM co-deposited films. The molar ratio of the TCTA to the

B3PYMPM of the TCTA:B3PYMPM co-deposited film is 1:1. The PL emission peaks of the TCTA, the B3PYMPM and the TCTA:B3PYMPM films are located at 393 nm, 396 nm and 492 nm, respectively. The PL emission peak of the TCTA:B3PYMPM is red-shifted from the TCTA or the B3PYMPM emission, and the energy of the TCTA:B3PYMPM emission peak is 2.5 eV. The energy level is similar to the difference between the HOMO level of the TCTA and the LUMO level of the B3PYMPM, proving that the TCTA and the B3PYMPM molecules form the exciplex upon excitation. In addition, the emission peaks of the TCTA and the B3PYMPM do not appear in the PL spectrum of the TCTA:B3PYMPM film, indicating that all the excitons in the TCTA:B3PYMPM film form the exciplexes. The PL efficiency of the TCTA-B3PYMPM exciplex was 36±2% at RT.

Characteristics of the exciplex can be understood from transient PL. Figure 4.2a shows the transient PL decay curves of the TCTA:B3PYMPM film at various temperatures. The transient PL decay of the exciplex showed delayed emission. The decay time of the delayed emission is on the order of μs. Although the lifetime of the singlet exciplex is generally longer than the singlet exciton, still the lifetime of the singlet exciplex is mostly shorter than 100 ns.[30,31] This long decay time of the delayed emission observed in this study indicates that the triplet exciplex participates in the light emission. The

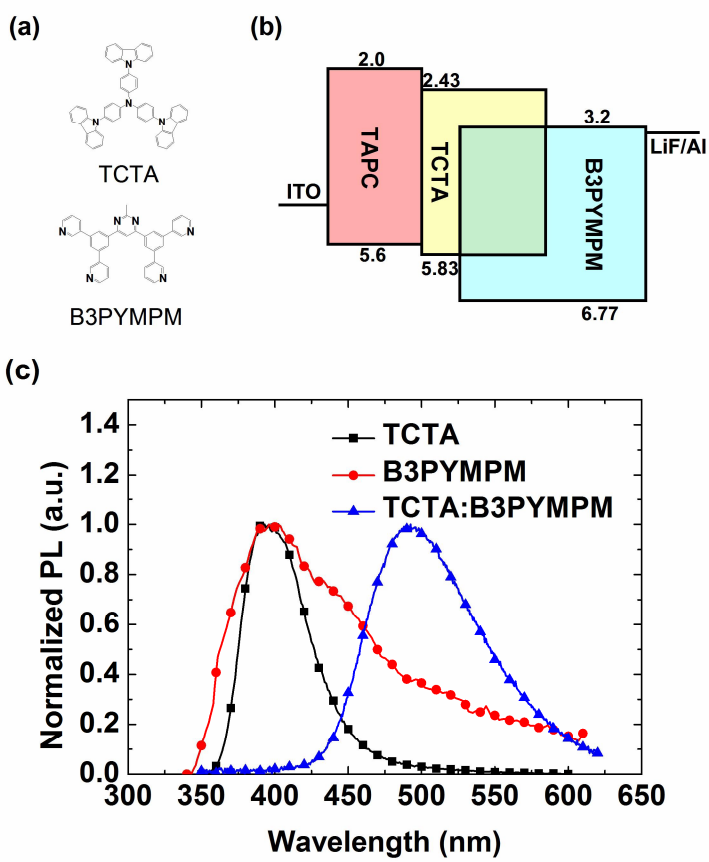

Figure 4.1 (a) Molecular structure of the TCTA and the B3PYMPM. (b) Device structure of the OLEDs using the TCTA-B3PYMPM exciplex. (c) Normalized PL spectra of the TCTA, the B3PYMPM and the TCTA:B3PYMPM co-deposited films.

intensity of the delayed emission of the exciplex increased as the temperature decreased, indicating that more triplet exciplexes were harvested as the temperature decreased.

Figure 4.2b and 4.2c shows the time resolve PL spectra of the TCTA:B3PYMPM co-deposited film at various delayed times. The PL spectra shifted to longer wavelengths with increasing delay time. At 300 K, the peak wavelength shifted from 484 nm to 530 nm. The spectrum shift of the exciplex was a continuous shift of the entire spectrum, not a change of the relative intensity between two emission peaks. This phenomenon is not observed in the TADF of single molecules.[7,8] The origin of the spectral shift is not very clear at this moment. Goushi *et al.* attributed the spectral shift to the time dependent variation of polarization in the host medium and the solvation effect.[25] Another plausible reason is the existence of a broad distribution of the energy level of the exciplex originating from different geometric arrangements between the two molecules forming the exciplex. As time goes on after the formation of the exciplex, the molecules forming the exciplex relax by molecular vibration and/or rotation to form a stable geometric arrangement. The relaxed stable geometry of the exciplexes can be different for different exciplexes because of the different local environments of the exciplexes in solid state. Low energy exciplexes must experience large

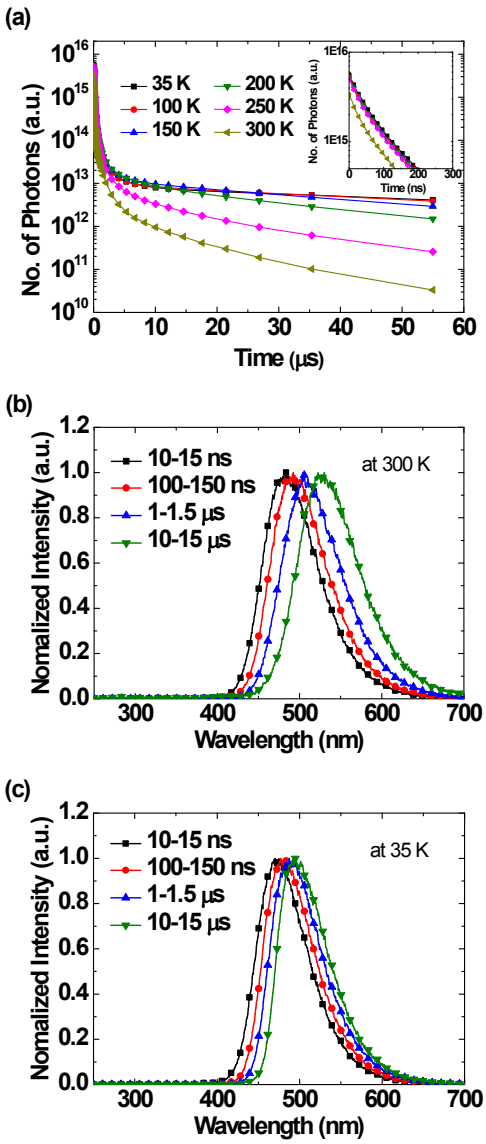

Figure 4.2 (a) Transient PL decay of the TCTA:B3PYMPM film at various temperatures. Inset: Enlarged image of the main graph. (b) Time resolved PL spectra of the TCTA:B3PYMPM film at various times after the excitation at 300 K. (c) Time resolved PL spectra of the TCTA:B3PYMPM film at various time after excitation at 35 K.

relaxation resulting in long delay time in emission and long lifetime of the triplet exciplex allows the exciplex to relax more so that the delayed emission gives more red shifted emission.

At low-T (35 K), the shift of the time resolved PL spectra of the exciplex with delayed time is smaller than that at higher temperature, and the wavelength of these spectra is shorter than that at higher temperature at same time scale, as shown in Figure 4.2c. The peak wavelength of the time resolved PL spectra at 35 K shifted from 470 nm to 495 nm. Because movements of the molecules are reduced at low-T, it is hard to fully relax to a stable geometric arrangement for the molecules which form the exciplex. Therefore, the exciplex showed a smaller emission peak shift and a higher energy emission. The PL efficiency of the TCTA:B3PYMPM film was measured using an integrating sphere and was 36% at RT. Using the PL efficiency at RT and the prompt and the delayed components of the transient PL intensity at various temperatures shown in Figure 4.2a, the PL efficiency of the TCTA:B3PYMPM film and the contribution of the prompt and the delayed components for the PL efficiency at various temperatures were extracted and they are shown in Figure 4.3. The PL efficiency increases rapidly as the temperature decreases, reaching to 90% at 200 K and 99% at 35 K. Observation of almost 100% PL efficiency from the exciplex emission is the first time to our best knowledge. Both the prompt

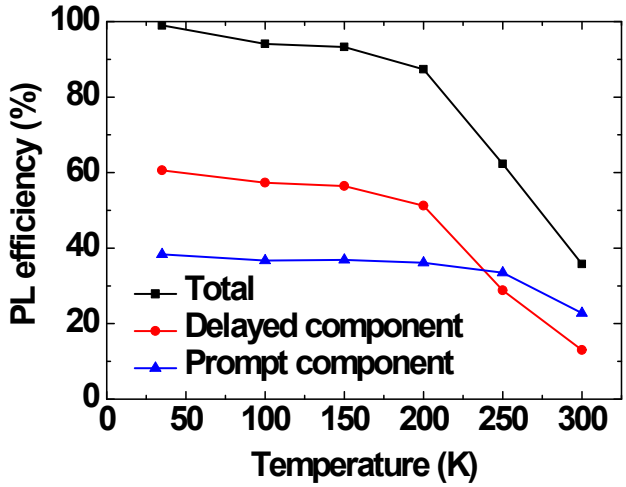

Figure 4.3 PL efficiency of the TCTA:B3PYMPM film and the contribution of the prompt and the delayed components for the PL efficiency at various temperatures.

and the delayed components increase as the temperature decreases. However, the increase of the delayed component is much larger than that of the prompt component, and it leads to the increase of the PL efficiency of the exciplex significantly with decreasing temperature. The large increase of the delayed component indicates that the RISC from the triplet exciplex to the singlet exciplex as well as the ISC from the singlet exciplex to the triplet exciplex is efficient.

Almost 100% PL efficiency and strong delayed emission at 35 K indicates that the non-radiative transition rate of the singlet and the triplet exciplex is zero. Delayed component of over 50% indicates that the ISC rate (k_{ISC}) is faster than the radiative decay rate of the singlet exciplex (k_r^S), where k_{ISC}=1.1x10^7 s^{-1} compared to k_r^S=7.0x10^6 s^{-1}. In the presence of the ISC and the RISC between the singlet and triplet states, the RISC rate (k_{RISC}) can be expressed as follows:[25]

$$k_{RISC} = \frac{k_p k_d}{k_{ISC}} \frac{\Phi_d}{\Phi_p}, \quad (1)$$

where k_p and k_d are the rate constants of the prompt and delayed fluorescence, Φ_p and Φ_d are the PL quantum efficiencies of the prompt and delayed components, respectively. The transient PL decay curves of the TCTA-

B3PYMPM exciplex shown in Figure 4.2a cannot be fitted with double exponential curves but correspond to a multi-exponential decay model. Therefore, k_d cannot be defined as a specific value, but rather has a range of $1x10^6$~$1x10^4$ s^{-1} depending on delay time. Then, the range of k_{RISC} can be calculated by using Equation 1. Figure 4.4 shows the range of k_{RISC} of the TCTA-B3PYMPM exciplex against temperature. The RISC rate has a distribution in the range of $3x10^6$~$3x10^4$ s^{-1} depending on the delay time (relaxation time of the exciplex) and is almost independent of temperature. The temperature independent RISC rate indicates that the RISC takes place without thermal activation. The broad range of the k_{RISC} may come from the broad energy level distributions of the singlet and the triplet exciplexes. Even with this slow k_{RISC}, the system has extremely low TTA allowing 100% PL efficiency. The energy level distribution and the low TTA will be discussed later (Figure 4.5 and 4.6).

Energetics of the singlet and the triplet exciplex in this system is not very clear at this moment. Goushi et al. reported the ΔE_{1-3} value of 50 meV from the Arrhenius plot of the RISC rate in an exciplex forming system.[25] In contrast, there are some reports that the singlet CT states nearly always lay energetically below the triplet CT states because exchange interaction of the CT states is dominated by kinetic exchange, which favors the singlet state,

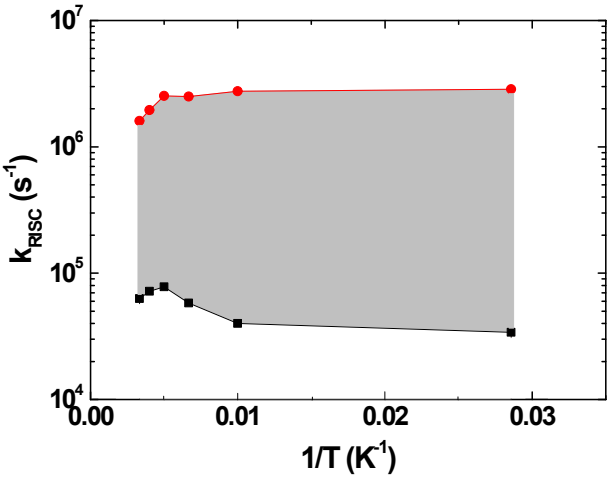

Figure 4.4 The range of the RISC rate of the TCTA:B3PYMPM film against the temperature. The square and circle indicate the minimum and maximum values of the RISC rate, respectively. The gray area indicates the range of the RISC rate.

due to short intermolecular distance and Coulombic interaction of the CT states.[11,12] Based on the shift of the emission spectrum with the delay time and the efficient ISC and RISC rates even at extremely low temperature of 35 K, we propose that the singlet and triplet exciplex have broad energy level distributions and the energy difference between them is extremely small that can be either positive or negative $\Delta E_{1\text{-}3}$ values, which is displayed schematically in Figure 4.5. The fact that the transient PL decay curves cannot be fitted with a double exponential curve but correspond to a multi-exponential decay model. It also supports this exciplex forming system has a broad distribution of $\Delta E_{1\text{-}3}$ values coming from the broad distributions of the singlet and the triplet exciplexes.

OLEDs were fabricated using the TCTA:B3PYMPM co-deposited film as the emitting layer, as shown in Figure 4.1b. The devices have a simple structure consisting of two hole transporting materials and one electron transporting material. The triplet energy of the TCTA and the B3PYMPM are higher than the energy of the exciplex[26,27] so that the energy transfer from the triplet exciplex to the materials is prevented. The current density-voltage-luminescence characteristics of the devices with different thick-nesses of the electron transporting layer are displayed in Figure 4.6a. The EL spectrum is close to the PL spectrum in Figure 4.1c as displayed in the inset of Figure 4.6b.

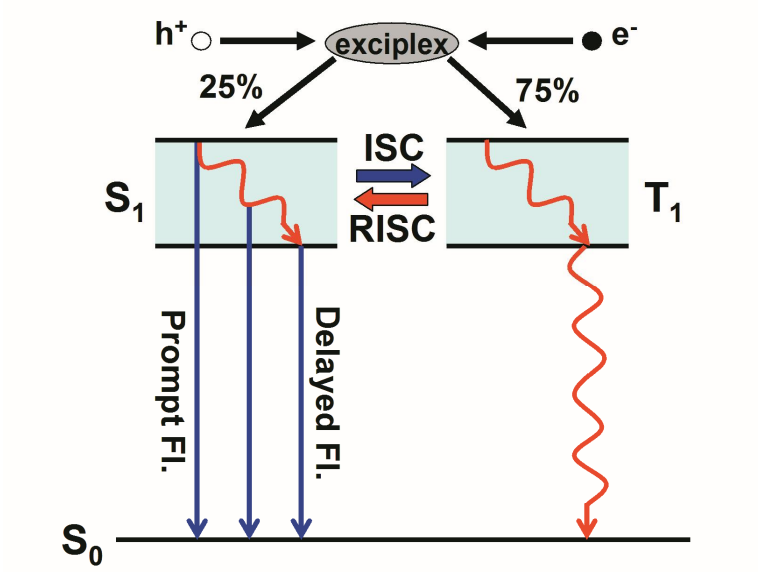

Figure 4.5 Schematic diagram of the delayed fluorescence mechanism by the RISC of the TCTA-B3PYMPM exciplex.

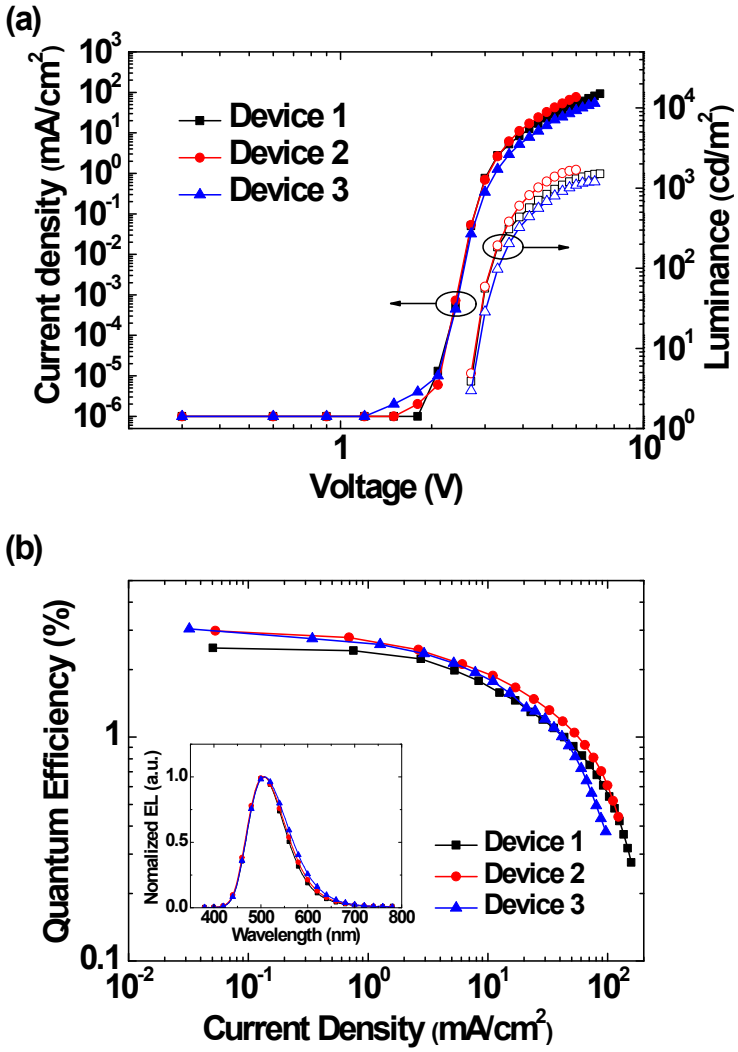

Figure 4.6 (a) Current density–voltage–luminance characteristics of the OLEDs. (b) EQE of the OLEDs as a function of the current density. Inset: EL spectra of the OLEDs at 6V.

It is interesting to note that the turn-on voltage of the devices is very low with a voltage of 2.7 V, close to the emitted photon energy, indicating that the potential drop for the charge injection and transport for the emission is minimal in this system, because there are only a minimal number of organic/organic junctions retarding the charge transport to the emission layer.

The EQE of the OLEDs using the TCTA-B3PYMPM exciplex are shown in Figure 4.6b. The maximum EQE of 3.1% was obtained from the device. The EQE is much higher than the expected value of 1.8%, considering the statistical ratio of the singlet excited state of 25%, the outcoupling efficiency of 20% and the PL efficiency of 36%, if only the singlet exciplex participates in the EL. This high efficiency of the OLEDs indicates that triplet exciplexes were harvested in the system.

Harvesting of the triplet exciplexes in the OLEDs is more clearly manifested by the transient EL decays at various current densities shown in Figure 4.7a. The transient EL exhibits long delayed emissions up to tens of μs. One plausible origin of the delayed emission is the TTA of the triplet exciplex. Since the TTA process involves second-order kinetics in terms of the concentration of the triplet excited states, the emission intensity of the delayed fluorescence by the TTA should be proportional to square of the current density if the formation of the triplet excited states is linearly proportional to

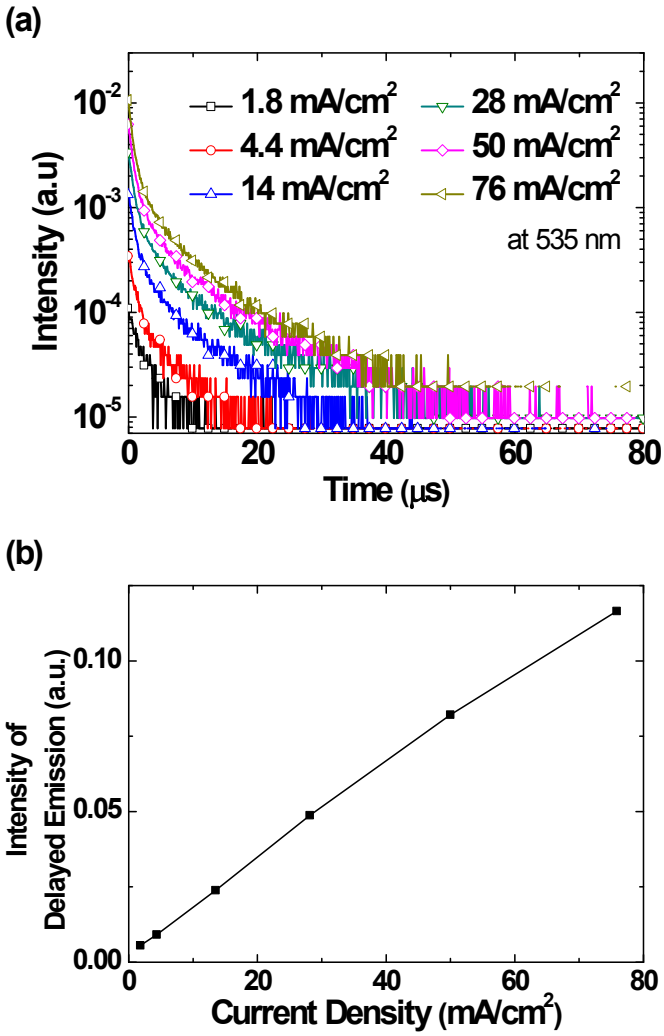

Figure 4.7 (a) Transient EL decay of device 2 at various current densities. (b) Intensity of the delayed EL emission of device 2 as a function of the current density.

the current density.[4] In contrast to the expectation, however, the intensity of the delayed EL emission of the OLED is linearly proportional to the current density, as shown in Figure 4.7b, demonstrating that the TTA of the exciplex is not the origin of the delayed emission of the OLED in the TCTA-B3PYMPM system. Therefore the RISC must be the origin of the delayed emission in the OLEDs. It is worth noting that the exciplex cannot diffuse because the exciplex forming materials have no absorption in the spectral range of the exciplex emission. Therefore, the collision probability between the two triplet exciplexes would be extremely low resulting in extremely low TTA.

The increase of the PL efficiency shown in Figure 4.3 resulted in the increase of the EQE of the OLEDs at low-T, as displayed in Figure 4.8. The current density is fixed at 0.1 mA/cm^2 in the measurements. The EQE of the OLED increased gradually with decreasing temperature, reaching to 10% at 195 K. The EQE value is the highest one to our best knowledge achieved using fluorescent molecule based exciplexes. Moreover the efficiency is two times higher than the theoretical limit of the EQE achievable with fluorescent molecules harvesting a singlet exciplex only, proving that triplet exciplexes are harvested to produce light in the system. The driving voltage increased from 2.8 V to 4.2 V as the temperature decreased from 300 K to 195 K, due to

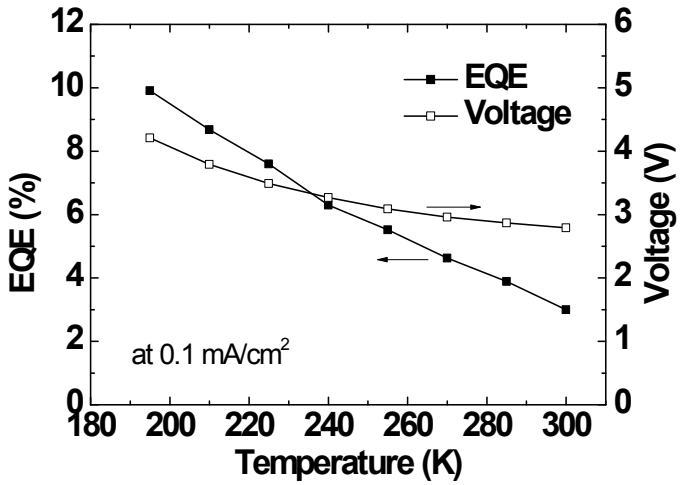

Figure 4.8 EQE and the driving voltage of device 2 at various temperatures (at 0.1 mA/cm^2).

the reduction of the mobility of the carriers with decreasing temperature.

4.4 Conclusion

Efficient triplet harvesting is demonstrated using an exciplex forming fluorescent molecular system, TCTA and B3PYMPM. The material system forms the exciplexes efficiently and shows the efficient delayed fluorescence emission. The delayed emission in-creased as the temperature decreased. As a result, the PL efficiency increased from 36% at RT to almost 100% at 35 K, and the EQE of the OLEDs increased from 3.1% to 10% at 195 K. The 10% EQE is the highest value obtained using exciplexes and clearly demonstrates that a large proportion of the triplet exciplexes are converted to light in the system. The time resolved PL spectra shifted to longer wavelengths with increasing delay time, indicating that the energy level of the exciplex has a broad distribution originating from different geometric arrangements between the two molecules forming the exciplex. Also, almost 100% PL efficiency showed efficient ISC and RISC rates even at extremely low temperature of 35 K, suggesting that the energy difference between them is extremely small. Therefore, the RISC from the triplet to singlet exciplex is possible in this system, even without thermal activation. The development of new exciplex

forming fluorescent material systems with low non-radiative process at RT must lead to a new way toward high efficiency OLEDs harvesting triplet energy to produce light using fluorescent molecules.

4.5 Bibliography

1. Y. Sun, N. C. Giebink, H. Kanno, B. Ma, M. E. Thompson, and S. R. Forrest, *Nature* **2006**, 440, 908
2. H.-J. Seo, K.-M. Yoo, M. Song, J. S. Park, S.-H. Jin, Y. I. Kim, and J.-J. Kim, *Org. Electron.* **2010**, 11, 564
3. S.-Y. Takizawa, J.-I Nishida, T. Tsuzuki, S. Tokito, and Y. Yamashita, *Inorg. Chem.* **2007**, 46, 4308
4. C. Ganzorig and M. Fujihira, *Appl. Phys. Lett.* **2002**, 81, 3137
5. A. Gerhard and H. Bässler, *J. Chem. Phys.* **2002**, 117, 7350
6. Y. Luo and H. Aziz, *Adv. Funct. Mater.* **2010**, 20, 1285
7. A. Endo, K. Sato, K. Yoshimura, T. Kai, A. Kawada, H. Miyazaki, and C. Adachi, *Appl. Phys. Lett.* **2011**, 98, 083302
8. A. Endo, M. Ogasawara, A. Takahashi, D. Yokoyama, Y. Kato, and C. Adachi, *Adv. Mater.* **2009**, 21, 4802
9. S. Park, O.-H. Kwon, Y.-S. Lee, D.-J. Jang, and S. Y. Park, *J. Phys. Chem. A* **2007**, 111, 9649
10. M. Klessinger, J. Michl, *Excited States and Photochemistry of Organic Molecules*, VCH, New York, U.S.A, **1995**
11. M. Segal, M. Singh, K. Rivoire, S. Diffley, T. Van Voorhis, and M. A.

Baldo, *Nat. Mater.* **2007**, 6, 374

12. S. Difley, D. Beljonne, and T. Van Voorhis, *J. Am. Chem. Soc.* **2008**, 130, 3420
13. W. M. Su, W. L. Li, Q. Xin, Z. S. Su, B. Chu, D. F. Bi, H. He, and J. H. Niu, *Appl. Phys. Lett.* **2007**, 91, 043508
14. N. Matsumoto, M. Nishiyama, and C. Adachi, *J. Phys. Chem. C* **2008**, 112, 7735
15. J. A. Osaheni and S. A. Jenekhe, *Macromolecules* **1994**, 27, 739
16. K. Itano, H. Ogawa, and Y. Shirota, *Appl. Phys. Lett.* **1998**, 72, 636
17. K. Okumoto and Y. J. Shirota, *J. Lumin.* **2000**, 87-89, 1171
18. G. Cheng, Y. Zhang, Y. Zhao, S. Liu, Z. Xie, H. Xia, M. Hanif, and Y. Mab, *Appl. Phys. Lett.* **2005**, 87, 013506
19. M. Li, W. Li, L. Chen, Z. Kong, B. Chu, B. Li, Z. Hu, and Z. Zhang, *Appl. Phys. Lett.* **2006**, 88, 091108
20. C. J. Liang and W. C. H. Choy, *Appl. Phys. Lett.* **2007**, 89, 251108
21. J. Feng, F. Li, W. Gao, S. Liu, Y. Liu, and Y. Wang, *Appl. Phys. Lett.* **2001**, 78, 3947
22. Q. J. Sun, B. H. Fan, Z. A. Tan, C. H. Yang, Y. F. Li, and Y. Yang, *Appl. Phys. Lett.* **2006**, 88, 163510
23. Q.-X. Tong, S.-L. Lai, M.-Y. Chan, J.-X. Tang, and H.-L. Kwong, *Appl.*

Phys. Lett. **2007**, 91, 023503

24. J. Kalinowski, M. Cocchi, D. Virgili, V. Fattori, and J. A. G. Williams, *Adv. Mater.* **2007**, 19, 4000
25. K. Goushi, K. Yoshida, K. Sato, and C. Adachi, *Nat. Photonics* **2012**, 6, 253
26. D. Tanaka, H. Sasabe, Y.-J. Li, S.-J. Su, T. Takeda, and J. Kido, *Jpn. J. Appl. Phys.* **2006**, 46, L10
27. S.-J. Su, E. Gonmori, H. Sasabe, and J. Kido, *Adv. Mater.* **2008**, 20, 4189
28. K. Noine, S. Kimura, Y.-J. Pu, K.-I. Nakayama, M. Yokoyama, and J. Kido, *J. Photopolym. Sci. Tech.* **2008**, 21, 323
29. W.-I. Jeong, S. Y. Kim, J.-J. Kim, and J. W. Kang, *Chem. Phys.* **2009**, 355, 25
30. A. C. Morteani, R. H. Friend, and C. Silva, *J. Chem. Phys.* **2005**, 122, 244906
31. N. Matsumoto, M. Nishiyama, and C. Adachi, *J. Phys. Chem. C* **2008**, 112, 7735

Chapter 5. Organic Light-emitting Diodes with Ultimate Efficiency using an Exciplex-Forming Co-host

5.1 Introduction

Recently, highly efficient organic light-emitting diodes (OLEDs) with external quantum efficiency (EQE) results of over 29% without any special structures of light extraction have been developed.[1,2] Presently however, the question arises of what the ultimate limit of the efficiency of an OLED is. There are three factors to consider in an evaluation of the efficiency of an OLED: the EQE, the driving voltage and the efficiency roll-off. A low driving voltage and a low efficiency roll-off (a high EQE at a high level of luminance) are especially important to reduce the power consumption in solid-state lighting, which requires high luminance and low power consumption.

Theoretical analysis showed that the ultimate limit of the EQE is about 30% for green phosphorescent OLEDs which can be obtained with a fairly thin transparent conducting electrode, emitters with 100% photoluminescence (PL) efficiency, optimized thickness of the organic layers and an optimized location

of the emitting zone in the OLEDs assuming isotropic emitter orientation[3].

Lower efficiency at high luminance in phosphorescent OLEDs has long been an issue in phosphorescent OLEDs, and triplet-triplet annihilation (TTA) and triplet-polaron quenching have been proposed as the origins of this issue.[4,5]

The driving voltage of an OLED must be composed of the voltage corresponding to the emitting photon energy ($V = E_{photon} / q$, where V is the voltage, E_{photon} is the photon energy of the emitted light and q is the unit charge) and the over-potential required to inject and transport electrons and holes from the electrodes to the emitting layer (EML), where the electrons and holes recombine. Therefore, the ultimate low limit of the driving voltage for highly efficient OLEDs must be close to the voltage corresponding to the photon energy of the light emitted by the OLED.[6] This can be obtained by minimizing the over-potential to drive the electrons and holes to the EML.

Among the three factors, the aforementioned experimental results reporting an EQE of 29% suggest that the EQE of OLEDs nearly reaches the theoretical limit, as obtained by innovative device structures and materials.[1,2] Unfortunately, however, the researchers failed to reach the ultimate limit of either the roll-off or the driving voltage.

The roll-off of the efficiency at high luminance can be reduced by lowering

the triplet-polaron quenching and the TTA. One approach to achieve low roll-off is to use a co-host system, which is supposed to have a broad emission zone to reduce the triplet and polaron density without them piling up in a narrow zone in the EML, but with limited success.[7-9] The roll-off is still high with a 15~35% reduction of the EQEs at 10,000 cd/m^2.

Approaches to lower the driving voltage are categorized as efforts that (1) lower the charge injection barrier between the electrode and the organic layer or between the organic layers, and (2) increase the charge carrier mobility of the organic layers. Electrical doping in the charge injection layer[10-24] and surface treatments of the indium tin oxide (ITO) anode[2,25-33] have been widely used to lower the injection barrier between the electrode and the organic layers. Given that the host in an EML must have a higher triplet energy than the phosphorescent dye, the energy gap between the highest occupied molecular orbital (HOMO) energy level and the lowest unoccupied molecular orbital (LUMO) energy level of the host is large so that there are significant energy barriers for electron and hole injections from the nearby hole transporting layer (HTL) and the electron transporting layer (ETL). One approach to overcome this problem is to use a co-host composed of a hole transporting material (HTM) and an electron transporting material (ETM).[7-9,34-40] In this system, electrons and holes reach the co-host EML without

energy barriers via the ETM and HTM, respectively.

However, if there is no interaction between the HTM and the ETM forming a co-host, there are two paths to form an exciton at the dopant molecules: direct charge trapping at the dopant sites to form the exciton at the dopant molecules, or formation of excitons at the HTM or the ETM molecules, followed by the energy transfer from the excitons to the dopants. Both mechanisms increase the driving voltage, resulting in diminishing the effect of the co-host to lower the voltage.

The exciplex-forming co-hosts proposed in this study are a system that overcomes all the barriers to realizing the ultimate efficiency in OLEDs in terms of the EQE, driving voltage and the efficiency roll-off. Figure 5.1 shows a schematic diagram of the device structure for the demonstration of an OLED which operates at the ultimate efficiency using an exciplex-forming co-host system. 4,4',4''-tris(N-carbazolyl)-triphenylamine (TCTA) and bis-4,6-(3,5-di-3-pyridylphenyl)-2-methylpyrimidine (B3PYMPM) were used as the HTM and ETM, respectively, forming an exciplex easily in an excited state with high PL efficiency.[41] The chemical structure and the energy levels of the molecules are also shown in Figure 5.1. The device has a very simple structure composed of three transporting materials and one phosphorescent emitting dye. There is only one organic/organic (O/O) junction with a HOMO

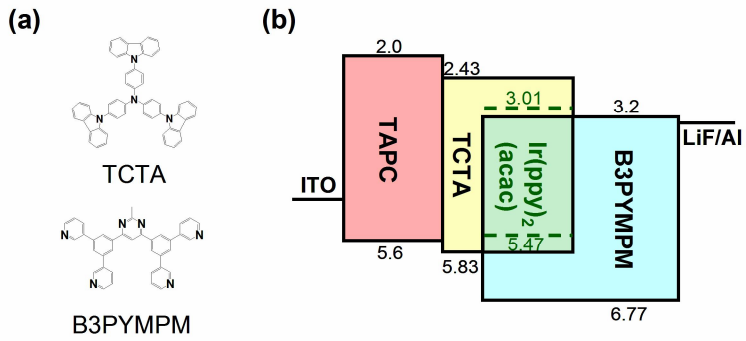

Figure 5.1 (a) The molecular structure of the TCTA and the B3PYMPM. (b) The device structure and energy level of the OLEDs.

level difference of only 0.2 eV for holes and no O/O junction for electrons to reach the EML in the device. Therefore, the over-potential to drive the electrons and holes to the EML after injection can be minimized. Moreover, the energy level difference between the LUMO of the ETM and the HOMO of the HTM is only 0.1 eV higher than the triplet energy gap of the dopant. Therefore, a very low turn-on voltage of the OLEDs as low as the triplet energy gap of the phosphorescent dopant can be achieved.[42]

In the TCTA-B3PYMPM co-host system, the holes at the TCTA molecules and the electrons at the B3PYMPM molecules form exciplexes easily; thus, the exciplexes transfer energy easily to the phosphorescent dopant of bis(2-phenylpyridine)iridium(III) acetylacetonate [$Ir(ppy)_2(acac)$].[43] Because of the easy formation of exciplexes in the EML by the recombination of electrons and holes, the polaron density in the EML is significantly lower than the injected charges, resulting in low triplet-polaron quenching in the OLEDs. Moreover, since the possibility of the triplet energy transfer from the dopant to nearby host molecules is very low, the triplet-triplet collision probability of the exciplex and the dopant is extremely low. In addition, the exciplex cannot diffuse because the exciplex forming materials have no absorption in the spectral range of the exciplex emission so that the collision probability between the two triplet exciplexes would be extremely low. Therefore, the

TTA of the exciplex-forming co-host system must be extremely small. All the factors contribute to increasing the EQE and reducing the efficiency roll-off of the OLEDs.

The OLED using the exciplex forming co-host showed an ultra-high EQE of 29.1%. This EQE value is close to the theoretical limit, as the outcoupling efficiency is limited by ~30% for general bottom-emission OLEDs without an outcoupling enhancement structure, assuming an isotropic emitter orientation.[3] Due to the low driving voltage and high EQE of the OLED, it reached a very high power efficiency of 124 lm/W. In addition, the roll-off of the efficiency of the OLED was extremely low with an EQE of 27.8% at 10,000 cd/m^2 and 26.0% at 20,000 cd/m^2.

5.2 Experimental

The OLEDs were fabricated by thermal evaporation onto cleaned glass substrates precoated with 70, 100 and 150-nm-thick ITO. Prior to the deposition of the organic layers, the ITO substrates were exposed to UV-ozone flux for 10 min following degreasing in acetone and isopropyl alcohol. All layers were grown by thermal evaporation at a base pressure of < 5×10^{-7} Torr without breaking the vacuum. The energy levels of the organic materials

were obtained from the published literature,[1,44,45] except for $Ir(ppy)_2(acac)$. The HOMO level of the $Ir(ppy)_2(acac)$ was obtained from cyclic voltammetry measurements. The LUMO level of the $Ir(ppy)_2(acac)$ was calculated from the HOMO level and the energy gap, which was obtained from the absorption spectrum.

The current density, the luminance, and the EL spectra were measured using a Keithley 2400 programmable source meter and a SpectraScan PR650 (Photo Research). The angular distribution of the EL intensity was measured using the Keithley 2400 programmable source meter, a rotation stage and an Ocean Optics S2000 fiber optic spectrometer. The EQE and the power efficiency of the OLEDs were calculated from the current density, the luminance, the EL spectra, and the angular distribution of the EL intensity data. The transient EL measurements were obtained by applying a 25 V electrical pulse with 200 ns width to the device and detecting the emission using a monochromator attached photomultiplier tube (PMT). Detection wavelength was 520 nm which corresponds to the peak wavelength of the $Ir(ppy)_2(acac)$ emission.

The organic films for the measurement of the PL spectra were fabricated by thermal evaporation on pre-cleaned quartz substrates at a base pressure of $< 5\times10^{-7}$ Torr. The PL spectra of the organic films were measured using an integrating sphere. A continuous-wave He/Cd laser (325 nm) was used as an

excitation light source and the monochromator attached PMT was used as an optical detector system. The low-temperature PL spectrum was measured in a cryostat, and the organic films were cooled down to 35 K. A pulsed Nd–YAG laser (355 nm) was used as the excitation light source and an intensified charge-coupled device (ICCD) was used as the optical detector for the measurements. For the transient PL measurement, the pulsed Nd–YAG laser (355 nm) was used as the excitation light source and the monochromator attached PMT was used as an optical detector system. The detection wavelength was 520 nm. The density of the initial excited states was calculated from the laser intensity, absorption coefficient of the film, area of the exciting spot, and the film thickness. The laser intensity was controlled by a neutral density filter.

The organic films for the measurement of the angle dependent PL were fabricated by thermal evaporation on pre-cleaned glass substrates at a base pressure of $< 5\times10^{-7}$ Torr. The experimental setup was composed with motorized rotation stage, half cylinder lens with holder of sample, dichroic mirror to filter the excitation beam, polarizer to classify the polarity of emitted light, fiber guided detector combined with the PMT and the monochromator. The He-Cd laser (CW type, 325 nm) used as the excitation source of the sample. The detection wavelength was 520 nm.

The calculation scheme of the outcoupling efficiency is referred from previous reported literatures[3,46,47]. The optical constants of organic layers excepting for B3PYMPM were measured by spectroscopic ellipsometer and those of the B3PYMPM, glass substrate, ITO and Al are referred from literatures[48-50].

5.3 Result and Discussion

Figure 5.2a shows the normalized PL spectra of the TCTA, the B3PYMPM and the TCTA:B3PYMPM co-deposited films. The molar ratio of the TCTA to the B3PYMPM in the co-deposited film was 1:1. The PL emission peak of the TCTA:B3PYMPM was red-shifted from the TCTA or the B3PYMPM emission, and the energy of the TCTA:B3PYMPM emission peak was 2.5 eV. This energy is similar to the difference between the HOMO level of the TCTA and the LUMO level of the B3PYMPM, proving that the TCTA and the B3PYMPM molecules form the exciplex upon excitation. In addition, the emission peaks of the TCTA and the B3PYMPM did not appear in the PL spectrum of the TCTA:B3PYMPM film, indicating that all of the excitons in the TCTA:B3PYMPM film form exciplexes effectively. The PL efficiency of the TCTA:B3PYMPM exciplex is 36±2%.[41] The PL spectrum of the

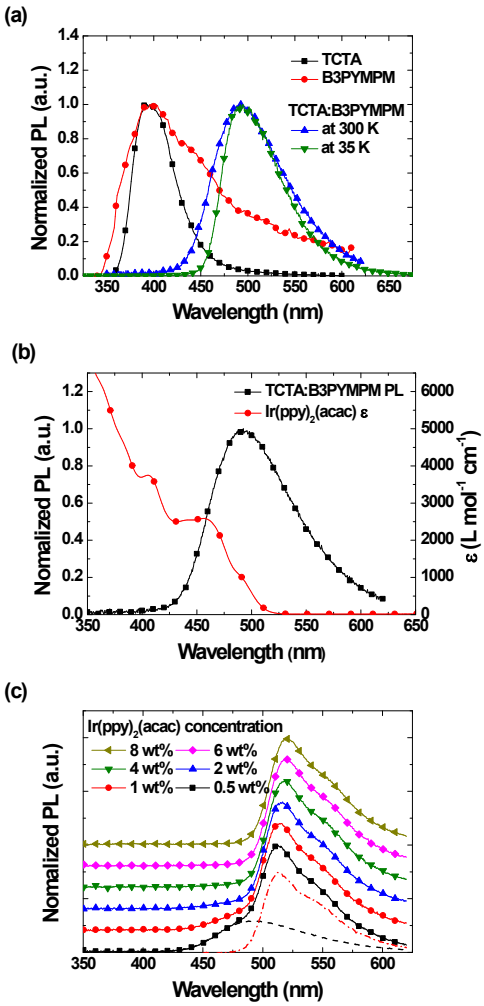

Figure 5.2 (a) The normalized PL spectra of the TCTA, the B3PYMPM and the TCTA:B3PYMPM co-deposited films. (b) The normalized PL spectrum of the TCTA:B3PYMPM co-deposited film and the extinction coefficient of the $Ir(ppy)_2(acac)$. (c) The normalized PL spectra of the $Ir(ppy)_2(acac)$ doped TCTA:B3PYMPM films at various doping concentrations. The PL spectrum of the 0.5 wt% $Ir(ppy)_2(acac)$-doped TCTA:B3PYMPM film is resolved into the TCTA-B3PYMPM exciplex emission (dashed line) and the $Ir(ppy)_2(acac)$ emission (dash-dot line).

TCTA:B3PYMPM film at a low temperature (35K) is also presented in Figure 5.2a. The emission peak of the PL spectrum of the TCTA:B3PYMPM film at the low temperature was very similar to that at room temperature, indicating that the singlet energy level (S_1) and the triplet energy level (T_1) of the TCTA-B3PYMPM exciplex are very similar. The exciplex is a type of intermolecular donor-acceptor system such that the orbital overlap between the excited state and the ground state is very small. Therefore, the exciplex is expected to have a very small energy difference between the singlet and the triplet excited states.[41,51]

The absorption spectrum of the phosphorescent dopant is compared in Figure 5.2b with the emission spectrum of the TCTA-B3PYMPM exciplex. $Ir(ppy)_2(acac)$ (T_1=2.4 eV) serves as the dopant, with a lower T_1 level than the TCTA, the B3PYMPM and the TCTA-B3PYMPM exciplex (T_1=2.76, 2.75 and 2.5 eV, respectively). The overlap between the PL spectrum of the TCTA-B3PYMPM exciplex and the absorption of the $Ir(ppy)_2(acac)$ is quite large; hence, the energy transfer from the exciplex to the $Ir(ppy)_2(acac)$ would be efficient. The Föster transfer radius from the exciplex to the $Ir(ppy)_2(acac)$ calculated from the data was 5.6 nm, which is quite long.[52] The energy transfer from the TCTA-B3PYMPM exciplex to the $Ir(ppy)_2(acac)$ was confirmed from the PL spectra of the $Ir(ppy)_2(acac)$-doped TCTA:B3PYMPM

films at various doping concentrations (Figure 5.2c). The exciplex emission peak appeared at low doping concentrations. However, the exciplex emission peak was eliminated when the concentration of the $Ir(ppy)_2(acac)$ was over 4 wt%, indicating that the energy transfer from the exciplex to the $Ir(ppy)_2(acac)$ under the photoexcitation is complete when the doping concentration exceeds 4 wt%.

The OLEDs shown in Figure 5.1 were fabricated using the TCTA-B3PYMPM co-host of the EML (Series A). The device structure of the series A OLEDs is as follows: indium tin oxide (ITO) (100 nm) / 1,1-bis-(4-bis(4-methyl-phenyl)-amino-phenyl)-cyclohexane (TAPC) (30 nm) / TCTA (10 nm) / TCTA:B3PYMPM:$Ir(ppy)_2(acac)$ (30 nm) / B3PYMPM (40 nm) / LiF (0.7 nm) / Al (100 nm). The molar ratio of the TCTA to the B3PYMPM of the EML was 1:1 and the doping concentration of the $Ir(ppy)_2(acac)$ varied from 2 wt% to 8 wt%. Figure 5.3a shows the current density-voltage-luminance characteristics of the series A OLEDs. The driving voltage of the OLEDs was mostly unchanged as the doping concentration increased. The driving voltage at 1 mA/cm^2 varied by no more than 0.03 V as the doping concentration changed from 2 wt% to 8 wt%, indicating that the probability of the direct trapping of the charges at the dopant site and the charge transporting through the dopants is low in the OLEDs. If charge trapping and transporting by the

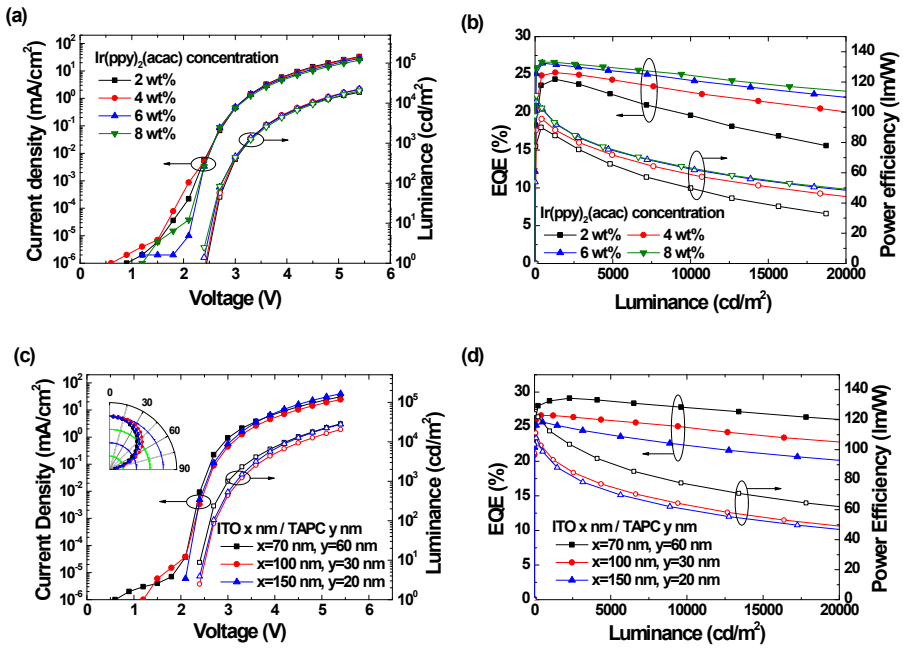

Figure 5.3 (a) The current density-voltage-luminance characteristics of the series A OLEDs. (b) The EQE and the power efficiency of the series A OLEDs. (c) The current density-voltage-luminance characteristics of the series B OLEDs. Inset: The angular distribution of the EL intensity of the series B OLEDs. Solid line represents Lambertian distribution. (d) The EQE and the power efficiency of the series B OLEDs.

dopants are dominant, the driving voltage of the OLEDs will be increased as the doping concentration increases up to the critical concentration due to the trapping effect of the dopant.[53] The turn-on voltage of the OLEDs was 2.4 V, which is as low as the triplet energy gap (2.4 eV) of the phosphorescent dopant, $Ir(ppy)_2(acac)$. In addition, the driving voltages of the OLEDs at 1,000 cd/m^2 and 10,000 cd/m^2 were 3.2 V and 4.4~4.6 V, respectively. The low turn-on voltage and over-potentials to drive the high carrier density to the EML of the OLEDs can be achieved because the exciplex forming co-host system has no charge injection barrier from the charge transporting layers to the emitting layer. This allows efficient formation of exciplexes, followed by the energy transfer from the exciplexes to the dopant molecules with a low probability of the direct trapping of the charges at the dopant molecules.

Figure 5.3b shows the EQEs and the power efficiencies of the series A OLEDs. These OLEDs showed high EQEs and low efficiency roll-offs. The efficiencies of the OLEDs were increased as the concentration of the $Ir(ppy)_2(acac)$ increased because a more efficient energy transfer from the exciplex to the dopant is possible as the concentration of the dopant increases. The OLED with 8 wt% $Ir(ppy)_2(acac)$ achieved a maximum EQE of 26.6%. In addition, the EQE of the OLED was 24.9% at 10,000 cd/m^2. The OLED also achieved a high power efficiency of 111.1 lm/W due to the low driving

voltage and the high EQE of the OLED.

The main limitation of the EQE of a phosphorescent OLED is the outcoupling efficiency. The thickness of the ITO can also affect the outcoupling efficiency of OLEDs.[3] Therefore, we fabricated OLEDs with various ITO thicknesses (Series B). The device structure of the series B OLEDs is as follows: ITO (x nm) / TAPC (y nm) / TCTA (10 nm) / TCTA:B3PYMPM:$Ir(ppy)_2(acac)$ (30 nm) / B3PYMPM (40 nm) / LiF (0.7 nm) / Al (100 nm). 70 nm, 100 nm and 150 nm thick ITOs were selected for this purpose, with the thickness of the TAPC varying accordingly from 60 nm to 20 nm to maximize the outcoupling efficiency. The molar ratio of the TCTA to the B3PYMPM of the EML was 1:1 and the doping concentration of the $Ir(ppy)_2(acac)$ in the EML was fixed at 8 wt%. Figure 5.3c shows the current density-voltage-luminance characteristics of the series B OLEDs. All the OLEDs in this work showed no EL spectrum shift with the driving voltage. The turn-on voltage of all the OLEDs was 2.4 V, which is as low as the triplet energy gap of the $Ir(ppy)_2(acac)$, and the driving voltage of the OLEDs at 1,000 cd/m^2 was 3.0~3.2 V. Again, such a low driving voltage can be achieved due to the charge injection barrier reduction by the co-host system and the energy transfer from the exciplex to the dopant. The inset of Figure 5.3c shows the angular distribution of the EL intensity of the series B OLEDs. The EQE and

the power efficiency of the series B OLEDs are shown in Figure 5.3d after calibration using the angular distribution of the emission intensity. The details of the performances of the OLEDs are summarized in Table 1. The OLED with 70-nm-thick ITO showed a very high EQE with a maximum EQE of 29.1%. This EQE value is close to the theoretical limit because the upper limit of the outcoupling efficiency is ~30% for general bottom-emission OLEDs without outcoupling enhancement structures assuming isotropic emitter orientation.

In recent study, however, the dipole orientation was expected with anisotropic dipole distribution in some material systems[48,54,55]. It is important that because outcoupling efficiency of horizontal dipoles is much higher than that of vertical dipoles. Thus, we examined the ratio of the dipole component by combining method of experimental work and theoretical analysis, and also predicted the outcoupling efficiency of the OLED based on the results. To analyze the dipole orientation, we measured and calculated the angle dependent PL. The sample for angle dependent PL measurement was TCTA (1 nm) / 8 wt% $Ir(ppy)_2(acac)$ doped TCTA:B3PYMPM (30 nm) which was thermally deposited on a glass substrate. We focused *p*-polarized light that both vertical and horizontal dipole orientations are emitted. After then, we calculated the angle dependent PL by classical electro-magnetic model that

Table 5.1 The details of the performances of the series B OLEDs

ITO	Voltage (V)		EQE (%)		Power efficiency (lm/W)	
thickness	Turn-on	@10000 cd/m^2	Max.	@10000 cd/m^2	Max.	@10000 cd/m^2
70 nm	2.4	5.1	29.2	27.6	119.5	63.0
100 nm	2.4	4.6	26.6	24.9	111.1	63.2
150 nm	2.4	4.3	25.7	22.3	107.8	60.2

the emission from exciton is considered as the power dissipated (or radiating) from oscillating dipole[46,56]. The calculated angle dependent PL were evaluated by combining *p*-polarized light of vertical and horizontal aligned dipole, which is following;

$$I_{PL} = xI_{\parallel} + (1-x)I_{\perp}, \quad (1)$$

where, I_{PL}, $I_{\parallel}$, and $I_{\perp}$ are the intensity of PL combined with light from vertical and horizontal aligned dipole, intensity of light from vertical and horizontal aligned dipole, respectively, and *x* is ratio of horizontal component of dipole. The fitting results were illustrated with experimental data in Figure 5.4. It showed that the ratio of dipole component is (horizontal:vertical) = (0.77:0.23) or (2:0.59).

We evaluated the outcoupling efficiency of our device structure, using this ratio of the dipole component. The calculation results of the outcoupling efficiency of the OLED according to the dipole orientation are demonstrated in 5.5. The outcoupling efficiency for the isotropic distribution is varied from 19.6% to 27.5% according to position of emission zone in the EML. On the other hands, the outcoupling efficiency varied from 25.1% to 32.5% when the fraction of the horizontally dipole is 0.77. The co-host system leads distribution of the electron-hole recombination zone overall EML[57]. Therefore,

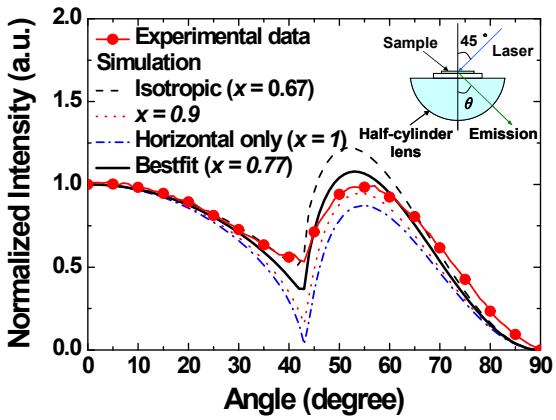

Figure 5.4 Measured *p*-polarized angle dependent PL emission pattern of the sample (TCTA (1 nm) / TCTA:B3PYMPM:8 wt% $Ir(ppy)_2(acac)$ (30 nm)). The wavelength of excitation laser is 325 nm and the detection wavelength is 520 nm. The black solid line is best fitting result compared with experimental data (x = 0.77). x indicates the ratio of the horizontal dipole component. Inset: Schematic diagram of the experimental geometry.

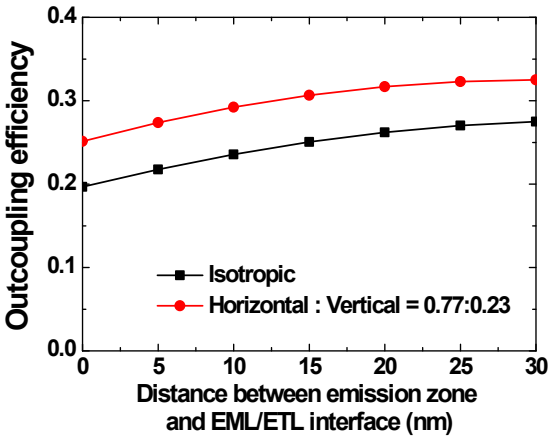

Figure 5.5 Calculated outcoupling efficiency of the OLED using TCTA:B3PYMPM co-host according to the dipole orientation of the emitter and the position of the emission zone.

we can assume emission zone of the OLED using TCTA:B3PYMPM co-host is distributed uniformly in the entire EML. Then, the outcoupling efficiency of the OLED would be about 29.8% which is average value of the outcoupling efficiency according to the emission zone position. This value is similar to the EQE of the OLED (29.1%). Hence, it indicates internal quantum efficiency of the OLED is almost maximized.

Additionally, the OLED achieved a very high power efficiency of 124.0 lm/W due to the low driving voltage and the high EQE of the OLED. This power efficiency approaches the ultimate efficiency of the OLEDs, as the driving voltage is close to the lower limit, which is the triplet energy gap of the phosphorescent-emitting dopant, and since the EQE approaches the higher limit, which is the limit of the outcoupling efficiency.

In addition, the EQE of the OLED was 28.7% at 1,000 cd/m^2, 27.8% at 10,000 cd/m^2 and 26.0% at 20,000 cd/m^2. Over 95% of the maximum EQE is maintained up to 10,000 cd/m^2 and about 90% at 20,000 cd/m^2. This low roll-off of efficiency is remarkable in phosphorescent OLEDs. The extremely low roll-off of the OLEDs indicates that the triplet-polaron quenching and the TTA are very low in the devices. Low triplet-polaron quenching can be easily understood by the low density of polarons in the exciplex forming co-host system as described in the transient EL measurements (Figure 5.6). In normal

non-exciplex forming co-host systems, the polaron density of the EML would be very high because the electrons and the holes are difficult to recombine at the host molecules; this is because of high energy level differences between the ETM and the HTM hosts. However, in the TCTA:B3PYMPM co-host system, electrons and holes in the EML form exciplexes very effectively as shown in Figure 5.2a resulting in significantly lower polaron density in the EML if the injected electrons and holes are well balanced.

Direct evidence of the energy transfer from the exciplexes to the dopant molecules and the low polaron density in the OLEDs under the electrical excitation can be obtained from the transient electroluminescence (EL) of the OLED. The structure of the devices for the transient EL measurement was as follow: ITO (70 nm) / TAPC (60 nm) / TCTA (10 nm) / EML [host:$Ir(ppy)_2(acac)$] (30 nm) / ETL (40 nm) / LiF (0.7 nm) / Al (100 nm). The host of the EML and the ETL of the device 1 were TCTA:B3PYMPM and B3PYMPM, and those of the device 2 were N,N'-dicarbazolyl-4-4'-biphenyl (CBP) and 1,3,5-tris (N-phenylbenzimidazole-2-yl)benzene (TPBi), respectively. The molar ratio of the TCTA to the B3PYMPM of the EML of the device 1 was 1:1 and the doping concentration of the $Ir(ppy)_2(acac)$ in the EML was 8 wt% for the both devices. The OLED using the CBP single host (device 2) was fabricated for comparison, and TPBi is used for ETL of the

OLED using CBP host because CBP and B3PYMPM forms exciplex at the interface.[43]

Figure 5.6 shows the transient EL decay of the OLEDs. The transient EL curve of the device 1 using the TCTA:B3PYMPM co-host showed increasing emission before decay. However, the transient EL decay of the device 2 using the CBP host showed almost single exponential decay right after the end of the excitation. The increasing emission before decay in the device 1 can be explained by the energy transfer from the host to the dopant. Considering the energy transfer from the host to the dopant, the rate equations of the excited states after excitation can be expressed as follows:

$$\frac{d[H^1]}{dt} = -k_H^1[H^1] - k_{ET}^1[H^1], \quad (2)$$

$$\frac{d[H^3]}{dt} = -k_H^3[H^3] - k_{ET}^3[H^3], \quad (3)$$

$$\frac{d[D^3]}{dt} = -k_D^3[D^3] + k_{ET}^1[H^1] + k_{ET}^3[H^3], \quad (4)$$

where $[H]$ and $[D]$ are the densities of the excited states of the host and the dopant, k_H and k_D are the decay rates of the host and the dopant, and k_{ET} is the energy transfer rate from the host to the dopant, respectively. The superscript '1' and '3' represent the singlet and triplet excited state, respectively. We assumed that the phosphorescent dopants emit light from the triplet excitons only due to the strong spin-orbit coupling. The coupled

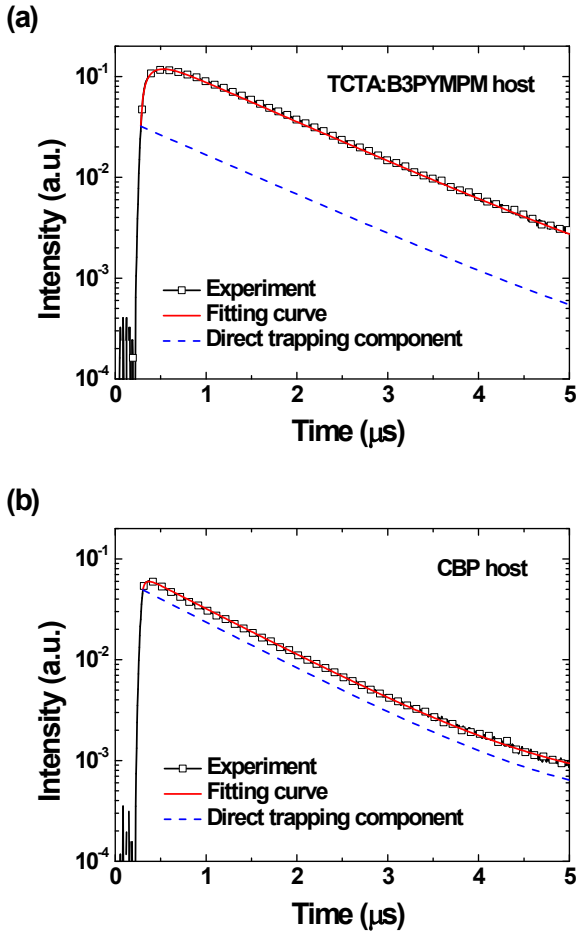

Figure 5.6 The transient EL decay curves of the OLEDs using (a) the TCTA:B3PYMPM co-host (device 1) and (b) the CBP host (device 2). The detection wavelength is 520 nm. Solid lines are the fitting curves of the transient EL decays and dashed lines are the transient EL curves by the direct trapping component only which were calculated using the Equation 5 and 6, respectively.

differential equations can be solved to

$$[D^3(t)] = -A_1 \exp[-(k_H^1 + k_{ET}^1)t] - A_2 \exp[-(k_H^3 + k_{ET}^3)t]$$

$$+ (A_1 + A_2 + [D^3(0)]) \exp(-k_D^3 t), \quad (5)$$

$$A_1 = \frac{k_{ET}^1 [H^1(0)]}{k_H^1 + k_{ET}^1 - k_D^3}, \quad A_2 = \frac{k_{ET}^3 [H^3(0)]}{k_H^3 + k_{ET}^3 - k_D^3},$$

where t is the time after excitation and $[D^3(0)]$, $[H^1(0)]$ and $[H^3(0)]$ are the number density of the excited states formed by direct trapping of charges at the dopant site, the number density of the singlet excited state and the triplet excited state of the host, respectively. Since the EL spectra of the OLEDs do not showed the emission from the host in both devices, we can safely that $k_H << k_{ET}$ and $k_H + k_{ET} \approx k_{ET}$. The above equation is converted to a single exponential decay (equation 6) if k_{ET} is zero as expected.

$$[D^3(t)] = [D^3(0)] \exp(-k_D^3 t). \quad (6)$$

The above analysis clearly shows that the increase of the transient EL curve after excitation comes from the energy transfer from the host exciplex to the dopant. Hence, the ratio of the emission coming from the energy transfer (r_{ET}) to the total emission can be represented as follows:

$$r_{ET} = \frac{[H^1(0)] + [H^3(0)]}{[D^3(0)] + [H^1(0)] + [H^3(0)]} \quad (7)$$

The transient EL curves were excellently fitted to Equation (5) as shown in Figure 5.6, and the parameters (k_{ET}^1, k_{ET}^3, k_D^3, and r_{ET}) obtained from the curve fittings are summarized in Table 2. The calculated transient EL curves by direct trapping component are also included in Figure 5.6. This analysis clearly shows that the energy transfer from the exciplex to the dopant molecules is the dominant mechanism of the light emission in the OLED with the TCTA:B3PYMPM co-host system doped with $Ir(ppy)_2(acac)$ even under the electrical excitation. 79% of the total emission comes from the energy transfer from the exciplex to the dopant in the device and only 21% comes from the direct trapping in the devicewith the TCTA:B3PYMPM host. The energy transfer probability is significantly higher than the $Ir(ppy)_2(acac)$ doped CBP single host system where only 25% of the emission comes from the energy transfer. This analysis clearly demonstrates that the host exciplexes are formed very effectively under the electrical excitation in the TCTA:B3PYMPM system doped with $Ir(ppy)_2(acac)$. This high density of the exciplex in the TCTA:B3PYMPM co-host naturally results in low polaron density in the EML to reduce the triplet-polaron quenching in the OLED using the TCTA:B3PYMPM co-host.

Table 5.2 Summary of the parameters extracted from the transient EL measurements of the OLEDs.

EML host	k_{ET}^{1} (s^{-1})	k_{ET}^{3} (s^{-1})	k_{D}^{3} (s^{-1})	r_{ET}
TCTA:B3PYMPM	3.1×10^{7}	7.6×10^{6}	9.1×10^{5}	0.79
CBP	7.7×10^{7}	2.3×10^{7}	1.1×10^{6}	0.25

It is interesting to note that the energy transfer rates of the singlet and the triplet excited states (k_{ET}^{1} and k_{ET}^{3}) of the CBP host are about 2~3 times faster than those of the TCTA:B3PYMPM co-host. It is expected because the overlap between the PL of the CBP and the absorption of the $Ir(ppy)_2(acac)$ is larger than the overlap between the PL of the TCTA:B3PYMPM exciplex and the absorption of the $Ir(ppy)_2(acac)$. However, the ratio of the emission coming from the energy transfer (r_{ET}) in the OLED using the TCTA:B3PYMPM co-host is much higher than the OLED using CBP host due to the higher density of the excited states in the TCTA:B3PYMPM system than the CBP host system.

The TTA process of the 8% $Ir(ppy)_2(acac)$ doped TCTA:B3PYMPM co-host system was analyzed using the transient PL decays shown Figure 5.7. It is interesting to note that the decay curves exhibit almost single-exponential decays independent of the exciplex density. These single exponential decays indicate that the TTA process is very slow in the system. The TTA process is quantitatively analyzed using the following equation which describes the decay of luminescence after short optical pulse excitation when the TTA process is included.[4,5]

$$L(t) = \frac{L(0)}{\{1 + [n_{ex}(0)]k_{TT}\tau/2\}e^{t/\tau} - [n_{ex}(0)]k_{TT}\tau/2}, \qquad (8)$$

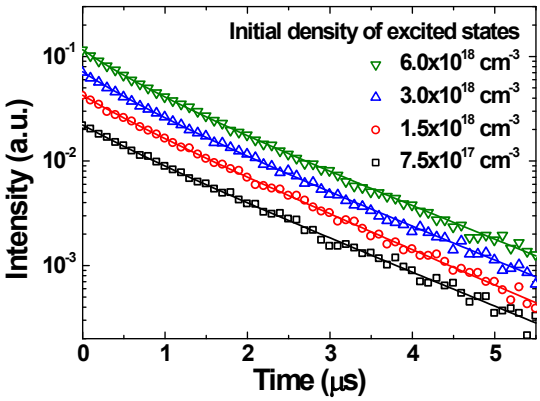

Figure 5.7 Transient PL decay of the TCTA:B3PYMPM:8%Ir(ppy)$_2$(acac) film at different excitation intensities indicated by the density of initial excited states. The wavelength of excitation laser is 355 nm and the detection wavelength is 520 nm. Solid lines represent calculated fits using Equation 8.

where t is the time after excitation, τ is the phosphorescent lifetime, $[n_{ex}(0)]$ is the density of the triplet excited state at t=0, k_{TT} is the rate constant of the TTA, and L is the luminescence intensity. Here, it is assumed that the luminescence intensity is linearly proportional to the concentration of excited states. The TTA rate constant (k_{TT}) and the lifetime (τ) extracted by the calculated fits of the transient PL decay curves are k_{TT} =(4±2)×10^{-19} cm^3/s and τ =1.34±0.04 μs, respectively. The TTA rate constant is negligibly small compared to that of phosphorescent dye doped single host films which are in the range of 10^{-10}~10^{-14} cm^3/s.[4,5,58,59] The triplet exciton of the dopant would be hardly transferred to triplet exciplex because the triplet energy levels of the host materials are much higher than that of the dopant (≥ 0.35 eV). Therefore, the collision probability between the triplet exciplex and the triplet exciton of the dopant would be extremely low, and it may be the reason of this extremely low TTA rate of the exciplex forming co-host system.

5.4 Conclusion

With the exciplex-forming TCTA-B3PYMPM co-host, we successfully developed a phosphorescent OLED with the ultimate low driving voltage,

high efficiency, and an extremely low efficiency roll-off. The TCTA-B3PYMPM co-host system removes the charge injection barrier from the charge transporting layers to the EML and allows an efficient single and triplet energy transfer from the exciplex to the dopant because the singlet and triplet energy of the exciplex are virtually identical. Therefore, the OLEDs achieved an extremely low turn-on voltage of 2.4 V, which is as low as the triplet energy gap of the phosphorescent-emitting dopant, and a very high EQE of 29.1%, which is close to the upper limit of the EQE for OLEDs without the outcoupling enhancement structure. In addition, due to the low driving voltage and high EQE of the OLEDs, they reach an ultimate power efficiency rating of 124.0 lm/W. The OLEDs also achieved an extremely low roll-off of efficiency due to low TTA and triplet-polaron quenching in the exciplex forming co-host system. The EQE of the optimized OLED remained over 27.8% up to 10,000 cd/m^2. This exciplex-forming co-host system represents a new method toward the creation of high-performance OLEDs.

5.5 Bibliography

1. D. Tanaka, H. Sasabe, Y.-J. Li, S.-J. Su, T. Takeda, and J. Kido, *Jpn. J. Appl. Phys.* **2007**, 46, L10
2. M. G. Helander, Z. B. Wang, J. Qiu, M. T. Greiner, D. P. Puzzo, Z. W. Liu, and Z. H. Lu, *Science* **2011**, 332, 944
3. S.-Y. Kim and J.-J. Kim, *Org. Electron.* **2010,** 11, 1010
4. M. A. Baldo, C. Adachi, and S. R. Forrest, *Phys. Rev. B* **2000**, 62, 10967
5. S. Reineke, K. Walzer, and K. Leo, *Phys. Rev. B* **2007**, 75, 125328
6. The threshold voltages in some inorganic light emitting diodes (LEDs) are lower than the band gap of the semiconductors where the threshold voltage is related to the difference of Fermi levels in the *p*- and *n*-semiconductors. However the energy conservation rule simply says that the output optical energy cannot be larger than the input electrical energy so that the minimum driving voltage must be close to the emitted photon energy ($V=h\nu/q$) *as long as the quantum efficiency is 1*.
7. J. Lee, J.-I. Lee, J. Y. Lee, and H. Y. Chu, *Org. Electron.* **2009**, 10, 1529
8. K. S. Yook, S. O. Jeon, C. W. Joo, J. Y. Lee, M. S. Kim, H. S. Choi, S. J. Lee, C.-W. Han, and Y. H. *Org. Electron.* **2009**, 10, 681
9. N. Chopra, J. S. Swensen, E. Polikarpov, L. Cosimbescu, F. So, and A. B.

Padmaperuma, *Appl. Phys. Lett.* **2010**, 97, 033304

10. J. Blochwitz, M. Pfeiffer, T. Fritz, and K. Leo, *Appl. Phys. Lett.* **1998**, 73, 729
11. J. Kido and T. Matsumoto, *Appl. Phys. Lett.* **1998**, 73, 2866
12. W. Gao and A. Kahn, *Org. Electron.* **2002**, 3, 53
13. C.-I. Wu, C.-T. Lin, Y.-H. Chen, M.-H. Chen, Y.-J. Lu, and C.-C. Wu, *Appl. Phys. Lett.* **2006**, 88, 152104
14. C.-C. Chang, M.-T. Hsieh, J.-F. Chen, S.-W. Hwang, and C. H. Chen, *Appl. Phys. Lett.* **2006**, 89, 253504
15. K.-H. Yim, G. L. Whiting, C. E. Murphy, J. J. M. Halls, J. H. Burroughes, R. H. Friend, and J.-S. Kim, *Adv. Mater.* **2008**, 20, 3319
16. F. Wang, X. Qiao, T. Xiong, and D. Ma, *Org. Electron.* **2008**, 9, 985
17. T. Matsushima and H. Murata, *Appl. Phys. Lett.* **2009**, 95, 203306
18. D.-S. Leem, J.-H. Lee, J.-J. Kim, and J.-W. Kang, *Appl. Phys. Lett.* **2008**, 93, 103304
19. J. Meyer, S. Hamwi, S. Schmale, T. Winkler, H.-H. Johannes, T. Riedl, and W. Kowalsky, *J. Mater. Chem.* **2009**, 19, 702
20. J.-H. Lee, D.-S. Leem, and J.-J. Kim, *Org. Electron.* **2008**, 9, 805
21. J.-H. Lee, D.-S. Leem, H.-J. Kim, and J.-J. Kim, *Appl. Phys. Lett.* **2009**, 94, 123306

22. J.-H. Lee, D.-S. Leem, and J.-J. Kim, *Org. Electron.* **2010**, 11, 486

23. J.-H. Lee, H.-M. Kim, K.-B. Kim, and J.-J. Kim, *Org. Electron.* **2011**, 12, 950

24. J.-H. Lee, H.-M. Kim, K.-B. Kim, R, Kabe, P. Anzenbacher Jr., and J.-J. Kim, *Appl. Phys. Lett.* **2011**, 98, 173303

25. Q.T. Le, F. Nuesch, L.J. Rothberg, E.W. Forsythe, and Y. Gao, *Appl. Phys. Lett.* **1999**, 75, 1357

26. K. Sugiyama, H. Ishii, Y. Ouchi, and K. Seki, *J. Appl. Phys.* **2000**, 87, 295

27. M. Ishii, T. Mori, H. Fujikawa, S. Tokito, and Y. Taga, *J. Lumin.* **2000**, 87-89, 1165

28. S. F. J. Appleyard, S. R. Day, R. D. Pickford, and M. R. Willis, *J. Mater. Chem*, **2000**, 10, 169

29. Y. Shen, D. B. Jacobs, G. G. Malliaras, G. Koley, M. G. Spencer, and A. Ioannidis, *Adv. Mater.* **2001**, 13, 1234

30. C. Qiu, Z. Xie, H. Chen, M. Wong, and H. S. Kwok, *J. Appl. Phys.* **2003**, 93, 3253

31. C. N. Li, C. F. Kwong, A. B. Djurišić, P. T. Lai, P. C. Chui, W. K. Chan, S. Y. Liu, *Thin Solid Films* **2005**, 477, 57

32. A. Sharma, P. J. Hotchkiss, S. R. Marder, and B. Kippelen, *J. Appl. Phys.* **2009**, 105, 084507

33. P. Cusumano, *Solid State Electron.* **2009**, 53, 1056

34. S. W. Liu, C. A. Huang, J. H. Lee, K. H. Yang, C. C. Chen, Y. Chang, *Thin Solid Films* **2004**, 453-454, 312

35. M. Cocchi, D. Virgili, V. Fattori, D. L. Rochester, and J. A. G. Williams, *Adv. Funct. Mater.* **2007**, 17, 285

36. M. E. Kondakova, T. D. Pawlik, R. H. Young, D. J. Giesen, D. Y. Kondakov, C. T. Brown, J. C. Deaton, J. R. Lenhard, and K. P. Klubek, *J. Appl. Phys.* **2008**, 104, 094501

37. X. Yang, Z. Wang, S. Madakuni, J. Li, and G. E. Jabbour, *Adv. Mater.* **2008**, 20, 2405

38. H.-H. Chou, H.-H. Shih, and C.-H. Cheng, *J. Mater. Chem.* **2010**, 20, 798

39. S. Lee and C. W. Tang, *J. Vac. Sci. Technol. B* **2011**, 29, 062401

40. K.-R. Wee, A.-L. Kim, S.-Y. Jeong, S. Kwon, and S. O. Kang, *Org. Electron.* **2011**, 12, 1973

41. Y.-S. Park and J.-J. Kim, *Angew. Chem. Int. Ed.* (submitted).

42. Kondakova *et. al.* previously reported OLEDs using TCTA:TPBi co-host system which shows exciplex emission (Ref. 36). However, PL efficiency of the TCTA-TPBi exciplex is very low, and the structures of the devices are complicated and have many O/O junctions. Therefore, these OLEDs could not fully utilize the advantage of the exciplex-forming co-host.

43. Y.-S. Park, W-I. Jeong, and J.-J. Kim, *J. Appl. Phys.* **2011**, 110, 124519

44. S.-J. Su, E. Gonmori, H. Sasabe, and J. Kido, *Adv. Mater.* **2008**, 20, 4189

45. K. Noine, S. Kimura, Y.-J. Pu, K.-I. Nakayama, M. Yokoyama, and J. Kido, *J. Photopolym. Sci. Tech.* **2008**, 21, 323

46. R. R. Chance, A. Prock, and R. Silbey, *Molecular Fluorescence and Energy Transfer Near Interfaces*, John Wiley & Sons, Inc., **1978**.

47. W.-I. Jeong, S.-Y. Kim, J.-J. Kim, and J.W. Kang, *Chem. Phys.* **2009**, 355, 25

48. D. Yokoyama, H. Sasabe, Y. Furukawa, C. Adachi, and J. Kido, *Adv. Funct. Mater.* **2011**, 21, 1375

49. E. D. Palik and G. Ghosh, *Handbook of optical constants of solids*, Academic Press, San Diego, **1998**

50. R. A. Synowicki, *Thin Solid Films*, **1998**, 313, 394

51. K. Goushi, K. Yoshida, K. Sato, and C. Adachi, *Nature Photonics* **2012**, 6, 253

52. T. Förster, *Discuss. Faraday Soc.* **1959**, 27, 7

53. L. Zhang, B. Li, L. Zhang, S. Yue, Q.Xue, and S. Liu, *J. Electrochem. Soc.* **2011**, 158, J243

54. J. Frischeisen, D. Yokoyama, C. Adachi, W. Brutting, *Appl. Phys. Lett.* **2010**, 96, 073302

55. M. Flammich, J. Frischeisen, D. S. Setz, D. Michaelis, B. C. Krummacher, T. D. Schmidt, W. Brutting, N. Danz, *Org. Electron.* **2011**, 12, 1663

56. J. A. E. Wasey, W. L. Barnes, *J. Mod. Optic.* **2000**, 47, 725

57. J. Lee, J.-I. Lee, J. Y. Lee, and H. Y. Chu, *Appl. Phys. Lett.* **2009**, 94, 193305

58. W. Holzer, A. Penzkofer, and T. Tsuboi, *Chem. Phys.* **2005**, 308, 93

59. S. Reineke, T. C. Rosenow, B. Lüssem, and K. Leo, *Adv. Mater.* **2010**, 22, 3189

초 록

이 논문은 크게 두 부분으로 구성되었다; (1) 호스트 물질보다 높은 에너지 준위를 갖는 새로운 녹색 도판트 물질을 사용하여 높은 효율과 색 안정성을 갖는 백색 유기발광소자 제작에 대한 연구와 (2) 엑시플렉스를 형성하는 물질 조합을 이용한 고효율의 유기발광소자에 대한 연구로 구성되어있다.

2장에서는 새롭게 합성한 녹색 도판트를 이용하여 높은 효율과 색 안정성을 갖는 백색 유기발광소자 제작에 대한 연구를 소개하였다. 이 백색 유기발광소자는 다중 발광층 구조의 소자로, 청색, 녹색, 적색 발광층의 순서로 구성되어 있다. 여기서 가운데 녹색 발광층의 도판트로 새로 합성한 tris-*fac*-(2-cyclohexenylpyridine) iridium(III) [$Ir(chpy)_3$] 또는 tris-*fac*-[2-(3-methylcyclohex-1-enyl)pyridine] iridium(III) [$Ir(mchpy)_3$] 라는 물질을 사용하였다. 이 도판트들은 호스트로 사용된 CBP보다 HOMO 레벨은 1.0~1.1 eV, LUMO 레벨은 0.3~0.4 eV 정도 높다. 이렇게 제작한 백색 유기발광소자는 11.7%의 높은 외부양자효율을 보였으며, 휘도가 10 cd/m^2에서 5,000 cd/m^2로 증가하는 동안 CIE 색좌표의 이동은 (0.02, 0.01) 미만으로 나타나 높은 색 안정성을 보임을 알 수 있었다. 이러한 백색 유기발광소자가 높은 효율과 색 안정성을 나타내는 것은 가운데 발광층의 호스트와 도판트

사이의 에너지 준위 차이가 각 발광층에서의 정공과 전자의 재결합 비율을 일정하게 유지시켜주는 역할을 하였기 때문으로 해석하였다.

3장에서는 유기발광소자의 발광층과 전자수송층 계면에서의 엑시플렉스 형성과 엑시플렉스에서 발광층의 도판트로의 에너지 전달에 대하여 분석하였다. 전자수송층으로 B3PYMPM를 사용하고, 발광층의 호스트로 CBP를 사용한 유기발광소자에서 B3PYMPM과 CBP가 형성한 엑시플렉스에 의한 발광을 확인할 수 있었다. 이러한 엑시플렉스 발광의 세기는 발광층의 도판트인 $Ir(ppy)_3$의 농도의 제곱에 반비례하는 모습을 보였으며, 이에 따라 소자의 발광 효율이 증가하였다. 이러한 현상은 엑시플렉스에서 도판트로의 에너지 전달에 의한 것으로 이를 Förster energy transfer mechanism을 이용하여 분석하였다. 또한, 이러한 계면에서의 엑시플렉스에서 도판트로의 에너지 전달을 이용하여 20.1%라는 높은 효율을 나타내는 유기발광소자를 제작하였다.

엑시플렉스는 전자주개와 전자받개가 결합한 형태이기 때문에 일중항과 삼중항의 에너지 차이가 매우 작을 수 있다. 4장에서는 이러한 특성을 이용하여 형광 물질로 이루어진 엑시플렉스에서 reverse intersystem crossing (RISC)를 통해 삼중항이 일중항으로 전환하여 빛을 발생시키는 연구를 하였다. TCTA와 B3PYMPM을 혼합한 시스템은 엑시플렉스를 효율적으로 형성하며, 지연발광을 나타낸다. 이러

한 지연발광은 삼중항에서 일중항으로 전환된 뒤 발광한 것으로 볼 수 있다. TCTA-B3PYMPM 엑시플렉스의 지연발광 효율은 온도가 낮아질수록 증가하는 모습을 보이는데, 그 결과 광발광 효율이 상온에서는 36%였으나, 35 K에서는 거의 100%로 나타났다. 또한 엑시플렉스를 이용한 유기발광소자의 외부양자 효율은 상온에서 3.1%, 195 K에서 10%로 나타났으며, 이는 삼중항 엑시플렉스의 상당부분이 일중항으로 전환되어 발광하였음을 의미한다. 온도에 따른 TCTA-B3PYMPM 엑시플렉스의 time resolved PL 스펙트럼과 transient PL을 분석하여 엑시플렉스의 에너지 준위가 넓은 분포를 갖고 있고, 일중항과 삼중항의 에너지 준위 차이가 매우 작음을 확인하였으며, 이는 삼중항 엑시플렉스가 일중항으로 전환이 가능하게 하는 요인이다.

5장에서는 엑시플렉스를 형성하는 두 물질을 발광층의 공동 호스트로 사용하여 외부양자효율, 구동 전압, 고휘도에서의 효율 측면에서 최고의 효율을 갖는 유기발광소자 제작에 대한 연구를 소개하였다. 공동 호스트를 이루는 두 물질은 각각 정공수송층과 전자수송층으로도 사용되기 때문에 전하수송층에서 발광층으로의 주입 장벽을 없앨 수 있다. 또한 엑시플렉스는 일중항과 삼중항의 에너지 차이가 매우 작기 때문에 도판트로 일중항과 삼중항 에너지를 모두 효율적으로 전달할 수 있다. 그리고 엑시플렉스 형성으로 인해 폴라론 밀도가 줄어들게 되고 도판트에서 엑시플렉스로는 삼중항 에너지 이

동이 어렵기 때문에 고휘도에서 인광 유기발광소자의 효율을 저하시키는 주된 원인인 triplet-polaron quenching과 triplet-triplet annihilation이 잘 일어나지 못하게 된다. 따라서 엑시플렉스를 형성하는 공동 호스트를 사용하면 높은 효율과 낮은 구동 전압을 얻을 수 있으며, 고휘도에서도 높은 효율을 유지할 수 있다. 본 연구에서는 엑시플렉스를 형성하는 두 물질 TCTA와 B3PYMPM을 공동 호스트로 사용하여 29.1%라는 매우 높은 외부양자효율과, 2.4 V라는 매우 낮은 구동 전압, 그리고 10,000 cd/m^{2}라는 높은 휘도에서도 최대 양자효율의 95% 이상을 유지하는 고성능의 유기발광소자를 제작하였다.

주요어: 백색 유기발광소자, 에너지 준위, 엑시플렉스, 에너지 전달, 공동 호스트

학 번: 2006-20844